

Rowan University

Rowan Digital Works


Theses and Dissertations

12-8-2017

Heterogeneous anisotropy index and scaling in multiphase random polycrystals

Muhammad Ridwan Murshed
Rowan University

Follow this and additional works at: <https://rdw.rowan.edu/etd>

 Part of the [Applied Mathematics Commons](#), [Materials Science and Engineering Commons](#), and the [Mechanical Engineering Commons](#)

Recommended Citation

Murshed, Muhammad Ridwan, "Heterogeneous anisotropy index and scaling in multiphase random polycrystals" (2017). *Theses and Dissertations*. 2486.
<https://rdw.rowan.edu/etd/2486>

This Dissertation is brought to you for free and open access by Rowan Digital Works. It has been accepted for inclusion in Theses and Dissertations by an authorized administrator of Rowan Digital Works. For more information, please contact graduateresearch@rowan.edu.

**HETEROGENEOUS ANISOTROPY INDEX AND SCALING IN
MULTIPHASE RANDOM POLYCRYSTALS**

by
Muhammad Ridwan Murshed

A Dissertation

Submitted to the
Department of Mechanical Engineering
College of Engineering
In partial fulfillment of the requirement
For the degree of
Doctor of Philosophy
at
Rowan University
October 25, 2017

Dissertation Chair: Shivakumar I. Ranganathan, Ph.D.

© 2017 Muhammad Ridwan Murshed

Dedication

To my family

Acknowledgements

First and foremost, I would like to thank my advisor Professor Shivakumar I. Ranganathan for his words of wisdom, constant encouragement, patience and guidance that immensely helped me shape up this dissertation. I will always remain highly indebted to him for strongly backing me during difficult times and for his ever-lasting support throughout this journey.

I wish to express my sincere gratitude to Professors Tirupathi R. Chandrupatla, Jennifer A. Kadlowec and Anthony F. Breitzman for serving on my dissertation committee. I would also like to thank them for their guidance, encouragement and long-lasting support during the course of my studies.

I am very thankful to Professors Martin Ostoja-Starzewski and Luis Costa for their constructive suggestions on my research.

I am extremely grateful to Dean Anthony M. Lowman for his support during my stay at Rowan. Also, I would like to thank the College of Engineering for providing the financial support that allowed me to pursue this research. In addition, I appreciate the staff for assisting me with various other matters. Special thanks to Rowan University and the Department of Mechanical Engineering for giving me this invaluable opportunity to enhance my knowledge and skills.

I am also thankful to all my teachers starting from primary school through graduate studies. Their mentorship and positive influence on me made this dissertation a reality.

I am very grateful to all my friends who have been extremely supportive throughout this journey.

Finally, I take this opportunity to thank my parents and my brother for their undying love and ever-lasting support.

Abstract

Muhammad Ridwan Murshed
HETEROGENEOUS ANISOTROPY INDEX AND SCALING IN MULTIPHASE
RANDOM POLYCRYSTALS
2017-2018
Shivakumar I. Ranganathan, Ph.D.
Doctor of Philosophy

Under consideration is the finite-size scaling of elastic properties in single and two-phase random polycrystals with individual grains belonging to any crystal class (from cubic to triclinic). These polycrystals are generated by Voronoi tessellations with varying grain sizes and volume fractions. By employing variational principles in elasticity, we introduce the notion of a ‘Heterogeneous Anisotropy Index (A_H^U)’ and investigate its role in the scaling of elastic properties at finite mesoscales (δ). The index A_H^U turns out to be a function of 43 variables, 21 independent components for each phase and the volume fraction of either phase. Furthermore, the relationship between A_H^U and the Universal Anisotropy Index, A^U is established for special cases. Rigorous scale-dependent bounds are then obtained by setting up and solving Dirichlet and Neumann type boundary value problems consistent with the Hill-Mandel homogenization condition. This leads to the concept of a dimensionless elastic scaling function which takes a power-law form in terms of A_H^U and δ . Based on the scaling function, a material scaling diagram is constructed using which one can estimate the number of grains required for homogenization. It is demonstrated that the scaling function quantifies the departure of a random medium from a homogeneous continuum.

Table of Contents

Abstract	v
List of Figures	ix
List of Tables	xi
Chapter 1: Introduction	1
1.1 Key Contributions	2
1.2 Overview of the Dissertation	3
Chapter 2: Methodology	4
2.1 Hill-Mandel Homogenization Condition	4
2.2 Elastic Scaling Function	7
2.2.1. Bounds on the Bulk and Shear Moduli	9
2.2.2. Homogenization Methodology	10
Chapter 3: Scaling Laws in Elastic Polycrystals With Individual Grains Belonging to Any Crystal Class	13
3.1 Introduction	13
3.2 Elastic Scaling Function	17
3.2.1. Properties and Bounds on the Elastic Scaling Function	20
3.3 Results and Discussion	20
3.3.1. Benchmark Results	21
3.3.2. Effect of Grain Shape on Scaling Function and Size of RVE	23
3.3.3. Bounds on the Aggregate Response	24

Table of Contents (Continued)

3.4 Constructing the Scaling Function	28	
3.5 Material Scaling Diagram	30	
3.6 Summary	33	
Chapter 4: Case Study: Hill-Mandel Condition and Bounds on Lower Symmetry Elastic Crystals.....		34
4.1 Introduction	34	
4.2 Methodology	36	
4.3 Results and Discussion	37	
4.4 Summary	39	
Chapter 5: Heterogeneous Anisotropy Index and Scaling in Two-Phase Random Polycrystals		40
5.1 Introduction	40	
5.2 Elastic Scaling Function.....	44	
5.2.1. Properties and Bounds on the Elastic Scaling Function	45	
5.2.2. Heterogeneous Anisotropy Index	46	
5.3 Results and Discussion	48	
5.3.1. Bounds on the Aggregate Response	49	
5.4 Constructing the Scaling Function.....	53	
5.5 Material Scaling Diagram	55	
5.6 Summary	58	

Table of Contents (Continued)

Chapter 6: Scaling Function in Mechanics of Random Materials	59
6.1 Introduction	59
6.2 Notion of a Scaling Function	60
6.2.1. Effect of Phase Contrast, k , on Scaling Function	61
6.2.2. Effect of Volume Fraction, v_f , on Scaling Function	62
6.2.3. Effect of an Anisotropy Measure, A , on Scaling Function	64
6.2.4. Effect of Mesoscale, δ , on Scaling Function	64
6.3 Application Problems	65
6.3.1. Conductivity in 2D Two-Phase Microstructures	66
6.3.2. Conductivity in 3D Polycrystals	67
6.3.3. Elasticity in 2D Two-Phase Checkerboards	67
6.3.4. Elasticity in 3D Polycrystals	68
6.3.5. Viscoelasticity in 2D Two-Phase Checkerboards	69
6.4 Summary	70
Chapter 7: Conclusions and Future Research Directions	71
References	73
Appendix: Author's Biography	82

List of Figures

Figure	Page
Figure 1. Methodology Flowchart	12
Figure 2. Generating a Polycrystal in Neper	12
Figure 3. Homogenization methodology for single phase elastic polycrystals	19
Figure 4. Comparison of grain shapes for Lithium	24
Figure 5. Bounds on elastic moduli of Cu (top), Zn (center) & SnF ₂ (bottom) ..	25
Figure 6. Bounds on elastic moduli of S (top), An ₉₆ (center) & Zr (bottom)	26
Figure 7. Bounds on elastic moduli of α Ti (top) & Fe ₂ O ₃ (bottom)	27
Figure 8. Scaling Function for single phase materials	28
Figure 9. Rescaled Scaling Function for single phase materials	29
Figure 10. Effective Rescaled Scaling Function & Fit for single phase materials .	30
Figure 11. Scaling Function & Fit for single phase materials	31
Figure 12. Contours of Scaling Function for $0.01 \leq f \leq 0.23$	32
Figure 13. Material Scaling Diagram at $f = 0.2$ (single phase materials)	32
Figure 14. A 10000-grain Voronoi tessellation	37
Figure 15. Homogenization methodology for two-phase elastic polycrystals	45
Figure 16. Heterogeneous Anisotropy Index (A_H^U) vs. Volume Fraction (v_f) for two-phase materials (Ni-Cd, Sn-Ag, Ni-Cr, Ni-Co)	47
Figure 17. Bounds on elastic moduli of Ni-Cd (top) and Sn-Ag (bottom) at various volume fractions	49

Figure 18. Bounds on elastic moduli of Ni-Cr (top) and Ni-Co (bottom) at various volume fractions	50
Figure 19. Scaling Function for two-phase materials	52
Figure 20. Rescaled Scaling Function for two-phase materials	53
Figure 21. Effective Rescaled Scaling Function & Fit for two-phase materials ...	54
Figure 22. Scaling Function & Fit for two-phase materials	56
Figure 23. Contours of Scaling Function for $0.01 \leq f \leq 0.23$	57
Figure 24. Material Scaling Diagram at $f = 0.2$ (two-phase materials)	57
Figure 25. Homogenization Methodology	60
Figure 26. $f_1(k)$ vs. Phase Contrast, k	63
Figure 27. $f_2(v_f)$ vs. Volume Fraction, v_f , in Electrical Conductivity	63
Figure 28. $f_4(\delta)$ vs. Mesoscale, δ , for several applications	70

List of Tables

Table	Page
Table 1. Materials analyzed across all crystal classes	22
Table 2. Model validation for shear modulus (GPa) of Cu (Dirichlet).....	22
Table 3. Model validation for shear modulus (GPa) of Cu (Neumann).....	22
Table 4. Bounds & self-consistent estimates (<i>SC</i>) of shear (μ) moduli (GPa)....	38
Table 5. Bounds & self-consistent estimates (<i>SC</i>) of bulk (κ) moduli (GPa)....	38
Table 6. Comparison of results using Hill-Mandel condition with self-consistent estimates for shear & bulk moduli (GPa)	39

Chapter 1

Introduction

Recent advances in computational mechanics have dramatically changed the landscape of engineering and science. The primary driving force is due to a rapid decrease in the computational cost which is estimated as a billion-fold reduction during the last 40 years (see Belytschko et al. [1]). In particular, computational mechanics has led to technological advancements in several areas including manufacturing, medicine, communication, defense, phenomena such as the movement of tectonic plates and astrophysics of black holes (see Oden et al. [2]).

A fertile ground of research within computational mechanics is the multiscale modeling of polycrystals. Such materials are widely used in engineering applications as the need to develop novel microstructures with unique properties has significantly increased (enhanced fracture toughness [3], high thermal conductivity [4], superior electrical conductivity [5]). Polycrystals consist of a collection of single crystals with individual grains belonging to any crystal class (from cubic to triclinic). When these crystals are oriented randomly, collectively they exhibit an effective elastic behavior that is isotropic upon ensemble averaging. However, despite advances in contemporary micromechanics over the past several decades, it is still a challenge to predict the effective properties of such polycrystals especially when the single crystals are highly anisotropic.

This dissertation focuses on scale-dependent homogenization of elastic polycrystals belonging to arbitrary crystal class. Homogenization is a widely used technique in the multiscale modeling of materials in which the macro-scale laws and the constitutive relations are determined by averaging over the micro-scale (see Mei and Vernescu [6]). There are two key issues which arise in the homogenization of random polycrystals: i) determining the apparent properties at finite length scales

(micro, meso, macro); and ii) the approach to a so-called Representative Volume Element (RVE). One powerful approach for estimating the effective property is to employ the Hill-Mandel [7, 8] homogenization condition. In this approach, the constitutive response of elastic polycrystals at finite scales is obtained by solving Dirichlet and Neumann type boundary value problems that bound the response from above and below, respectively. The microstructure is assumed to be spatially homogeneous, ergodic and with increasing length scales, the microstructure moves from a so-called Statistical Volume Element (SVE) to a Representative Volume Element (RVE). The versatility of this methodology is evident from the fact that it has attracted a great deal of interest over the past several decades within the context of elasticity [9, 10], thermal conductivity [11, 12], electrical conductivity [13], thermoelasticity [14, 15], flow in porous media [16, 17] and fracture and damage phenomena in random microstructures [18].

1.1 Key Contributions

The key contributions of this dissertation are as follows:

- a) Obtain scale-dependent bounds on the elastic response of single phase and two-phase random polycrystals.
- b) Employ Hill-Mandel condition to obtain bounds on highly anisotropic single crystals belonging to lower symmetry class.
- c) Introduce the notion of a scaling function and establish its functional form in terms of the single crystal properties and the mesoscale.
- d) Formulate the concept of a Heterogeneous Anisotropy Index, A_H^U , using variational principles in elasticity and tensor algebra in order to establish its relationship with the scaling function.
- e) Establish the analogy of scaling function to dimensionless numbers in continuum mechanics.

1.2 Overview of the Dissertation

In the subsequent sections, we consider the following:

- a) Chapter 2 discusses the methodology employed in this dissertation.
- b) Chapter 3 illustrates the scaling behavior of elastic random polycrystals (single phase) with individual grains belonging to any crystal class (from cubic to triclinic).
- c) Chapter 4 is a case study on determining the effective properties of polycrystals comprising of highly anisotropic single crystals belonging to lower symmetry class.
- d) Chapter 5 demonstrates the scaling behavior of two-phase polycrystals through the notion of Heterogeneous Anisotropy Index, A_H^U .
- e) Chapter 6 discusses the concept of a dimensionless scaling function and examines its role in the context of multiscale mechanics of random composites.
- f) The conclusions and future research directions are shown in Chapter 7.

Chapter 2

Methodology

The chapter focuses on the mathematical formulation that forms the basis for obtaining rigorous scale-dependent bounds. We begin by first introducing the Hill-Mandel homogenization condition and then develop the formulation for an elastic scaling function. Subsequently, the theory for scale-dependent bounds is discussed and the methodology for numerical implementation of the boundary value problems is presented.

2.1 Hill-Mandel Homogenization Condition

Consider the Cauchy stress, $\boldsymbol{\sigma}$, and infinitesimal strain, $\boldsymbol{\varepsilon}$, tensors and decompose them into the superposition of the means ($\overline{\boldsymbol{\sigma}}$ and $\overline{\boldsymbol{\varepsilon}}$) with zero-mean ($\boldsymbol{\sigma}'$ and $\boldsymbol{\varepsilon}'$) fluctuations (see Ostoja-Starzewski [18])

$$\begin{aligned}\boldsymbol{\sigma}(\omega, \mathbf{x}) &= \overline{\boldsymbol{\sigma}} + \boldsymbol{\sigma}'(\omega, \mathbf{x}), \\ \boldsymbol{\varepsilon}(\omega, \mathbf{x}) &= \overline{\boldsymbol{\varepsilon}} + \boldsymbol{\varepsilon}'(\omega, \mathbf{x}).\end{aligned}\tag{2.1}$$

Here \mathbf{x} is the point-to-point dependence of fluctuating fields, $\omega(\in \Omega)$ refers to a particular realization in a microstructure from the sample space, Ω , and over-bar is used to represent the volume average. For a specific realization, $B_\delta(\omega)$, of a random medium, B_δ , the volume average of the energy density can be defined as follows

$$\overline{U} \equiv \frac{1}{2V} \int_{B_\delta(\omega)} \boldsymbol{\sigma}(\omega, \mathbf{x}) : \boldsymbol{\varepsilon}(\omega, \mathbf{x}) dV = \frac{1}{2} \overline{\boldsymbol{\sigma} : \boldsymbol{\varepsilon}} = \frac{1}{2} \overline{\boldsymbol{\sigma}} : \overline{\boldsymbol{\varepsilon}} + \frac{1}{2} \overline{\boldsymbol{\sigma}' : \boldsymbol{\varepsilon}'},\tag{2.2}$$

where V is the volume of the microstructure. In Eq. (2.2), for the volume average of a scalar product of stress and strain fields to equal the product of their averages

$$\overline{\boldsymbol{\sigma} : \boldsymbol{\varepsilon}} = \overline{\boldsymbol{\sigma}} : \overline{\boldsymbol{\varepsilon}},\tag{2.3}$$

the fluctuations need to be zero as follows

$$\overline{\boldsymbol{\sigma}' : \boldsymbol{\varepsilon}'} = 0. \quad (2.4)$$

Eq. (2.3) is known as the Hill-Mandel homogenization condition. We now rewrite Eq. (2.4) in index notation as follows (see Ostoja-Starzewski [18])

$$\begin{aligned} \overline{\boldsymbol{\sigma}' : \boldsymbol{\varepsilon}'} &= \int_V (\sigma_{ij} - \bar{\sigma}_{ij})(\varepsilon_{ij} - \bar{\varepsilon}_{ij}) dV \\ &= \frac{1}{V} \int_V \left\{ [(\sigma_{ij} - \bar{\sigma}_{ij})(u_i - \bar{u}_i)]_{,j} - (\sigma_{ij,j} - \bar{\sigma}_{ij,j})(u_i - \bar{u}_i) \right\} dV \\ &= \frac{1}{V} \int_{\partial V} [(\sigma_{ij} - \bar{\sigma}_{ij})(u_i - \bar{u}_i)] n_j dS \\ &= \frac{1}{V} \int_{\partial V} [(t_i - \bar{\sigma}_{ij} n_j)(u_i - \bar{\varepsilon}_{ij} x_j)] dS, \end{aligned} \quad (2.5)$$

where u_i is the displacement vector, n_j is the outward unit normal and t_i is the uniform traction vector ($t_i = \sigma_{ij} n_j$). In the limit ($\delta \rightarrow \infty$), the fluctuations are negligible. But, for a specific mesoscale, the necessary condition for Eq. (2.3) to hold is (see Ranganathan and Ostoja-Starzewski [19])

$$\overline{\boldsymbol{\sigma} : \boldsymbol{\varepsilon}} = \bar{\boldsymbol{\sigma}} : \bar{\boldsymbol{\varepsilon}} \Leftrightarrow \int_{\partial B_\delta} (\mathbf{t} - \bar{\boldsymbol{\sigma}} \cdot \mathbf{n}) \cdot (\mathbf{u} - \bar{\boldsymbol{\varepsilon}} \cdot \mathbf{x}) dS = 0, \quad (2.6)$$

and ∂B_δ is the boundary of B_δ . By using Eq. (2.6), the three types of boundary conditions are defined as follows (see Ranganathan and Ostoja-Starzewski [19], Hill [20])

i) Uniform Displacement (Dirichlet)

$$\mathbf{u}(\mathbf{x}) = \boldsymbol{\varepsilon}^0 \cdot \mathbf{x}, \quad (2.7a)$$

ii) Uniform Traction (Neumann)

$$\mathbf{t}(\mathbf{x}) = \boldsymbol{\sigma}^0 \cdot \mathbf{n}, \quad (2.7b)$$

iii) Mixed-orthogonal

$$[\mathbf{t}(\mathbf{x}) - \sigma^0 \cdot \mathbf{n}] \cdot [\mathbf{u}(\mathbf{x}) - \varepsilon^0 \cdot \mathbf{x}] = 0. \quad (2.7c)$$

The material properties obtained using Eq. (2.7c) are always between the apparent moduli determined by applying Dirichlet and Neumann type boundary conditions (see Ostoja-Starzewski [18]). Also, the mixed-orthogonal boundary condition can represent an actual experimental setup where displacements are applied without friction on every side of the specimen under investigation (see Khisaeva and Ostoja-Starzewski [21]). It is now possible to set up stochastic boundary value problems with the above boundary conditions and upon ensemble averaging, the mesoscale effective response can be obtained.

The methodology outlined above holds true under the assumption that the microstructure is spatially homogeneous and ergodic for the random field, $\Theta(\omega, \mathbf{x})$, of material parameters involved. In particular, $\Theta(\omega, \mathbf{x})$ is a wide-sense stationary (WSS) random field with a finite-valued covariance and a constant mean (see Ostoja-Starzewski [15])

$$\begin{aligned} \langle \Theta(\mathbf{x}) \rangle &= \mu, \\ \langle [\Theta(\mathbf{x}) - \langle \Theta(\mathbf{x}) \rangle][\Theta(\mathbf{x} + \mathbf{h}) - \langle \Theta(\mathbf{x} + \mathbf{h}) \rangle] \rangle &= K_{\Theta}(\mathbf{h}) < \infty, \end{aligned} \quad (2.8)$$

where $K_{\Theta}(\mathbf{h})$ is the covariance function and the ensemble averages are represented by $\langle \cdot \rangle$. It can also be observed that the random field, $\Theta(\omega, \mathbf{x})$, outlined above is mean-ergodic if the spatial average (denoted by over-bar) is equal to the ensemble average (see Ostoja-Starzewski [15])

$$\langle \overline{\Theta} \rangle = \overline{\langle \Theta \rangle}. \quad (2.9)$$

In the next section, we postulate a generic form of the scaling function for random materials.

2.2 Elastic Scaling Function

Single crystals are elastically anisotropic and the extent of anisotropy is quantified by the Universal Anisotropy Index, A^U , defined as follows (see Ranganathan and Ostoja-Starzewski [22])

$$A^U = 5 \frac{G^V}{G^R} + \frac{K^V}{K^R} - 6. \quad (2.10)$$

Now, consider an arbitrary realization, $B_\delta(\omega)$, of a random medium, B_δ , on a specific mesoscale, δ . By using Eq. (2.7a), a mesoscale random stiffness tensor, \mathbf{C}_δ^d , can be defined as (see Ostoja-Starzewski [18])

$$\bar{\boldsymbol{\sigma}}_\delta(\omega) = \mathbf{C}_\delta^d(\omega) : \boldsymbol{\varepsilon}^0, \quad (2.11)$$

where superscript, d , is the displacement boundary condition (see Ostoja-Starzewski et al. [23]). Along similar lines, Eq. (2.7b) yields a mesoscale random compliance tensor, \mathbf{S}_δ^t , as follows (see Ostoja-Starzewski [18])

$$\bar{\boldsymbol{\varepsilon}}_\delta(\omega) = \mathbf{S}_\delta^t(\omega) : \boldsymbol{\sigma}^0, \quad (2.12)$$

and superscript, t , is the uniform traction boundary condition (see Ostoja-Starzewski et al. [23]). In general, \mathbf{C} and \mathbf{S} are anisotropic at finite mesoscales. Isotropic response can only be recovered by distributing the single crystal orientation randomly and upon ensemble averaging. The isotropic forms of the stiffness and compliance tensors in terms of the bulk modulus, K , as well as the shear modulus, G , can be represented as follows (see Ranganathan and Ostoja-Starzewski [10])

$$\langle \mathbf{C}_\delta^d \rangle = 2 \langle G_\delta^d \rangle \mathbf{K} + 3 \langle K_\delta^d \rangle \mathbf{J}, \quad (2.13a)$$

$$\langle \mathbf{S}_\delta^t \rangle = \frac{1}{2 \langle G_\delta^t \rangle} \mathbf{K} + \frac{1}{3 \langle K_\delta^t \rangle} \mathbf{J}, \quad (2.13b)$$

where \mathbf{J} and \mathbf{K} are the spherical and deviatoric components (introduced by Walpole [24, 25]) of the fourth order identity tensor, $\mathbf{I} = I_{ijkl} e_i \otimes e_j \otimes e_k \otimes e_l = \frac{\delta_{il}\delta_{jk} + \delta_{ik}\delta_{jl}}{2} e_i \otimes e_j \otimes e_k \otimes e_l$. In addition, δ_{ij} is the Kronecker δ with $\delta_{ij} = 1$ when $i = j$ and $\delta_{ij} = 0$ when $i \neq j$. Also, $\mathbf{J} = J_{ijkl} e_i \otimes e_j \otimes e_k \otimes e_l = \frac{\delta_{ij}\delta_{kl}}{3} e_i \otimes e_j \otimes e_k \otimes e_l$ and $\mathbf{K} = \mathbf{I} - \mathbf{J}$ (see Ranganathan et al. [26]). By quadruple contraction of Eqs. (2.13a) and (2.13b), the following scalar equation is obtained (see Itskov [27] and Ranganathan and Ostoja-Starzewski [10])

$$\langle \mathbf{C}_\delta^d \rangle :: \langle \mathbf{S}_\delta^t \rangle = 5 \frac{\langle G_\delta^d \rangle}{\langle G_\delta^t \rangle} + \frac{\langle K_\delta^d \rangle}{\langle K_\delta^t \rangle}, \quad (2.14)$$

where the contraction indicates identifying two indices and summing over them as dummy indices (see Holzapfel [28]). In the limit ($\delta \rightarrow \infty$), the stiffness tensor is the exact inverse of the compliance tensor as follows (see Ranganathan and Ostoja-Starzewski [10])

$$\lim_{\delta \rightarrow \infty} \langle \mathbf{C}_\delta^d \rangle :: \langle \mathbf{S}_\delta^t \rangle = 6. \quad (2.15)$$

Rearranging Eqs. (2.14) and (2.15), we postulate the following relationship

$$\langle \mathbf{C}_\delta^d \rangle :: \langle \mathbf{S}_\delta^t \rangle = \lim_{\delta \rightarrow \infty} \langle \mathbf{C}_\delta^d \rangle :: \langle \mathbf{S}_\delta^t \rangle + f(C^{ij}, \delta), \quad (2.16)$$

where $f(C^{ij}, \delta)$ is the dimensionless function called the elastic scaling function. The specific forms of scaling function for random materials will be discussed in the subsequent chapters of the dissertation. In the next section, we discuss the upper and lower bounds on the bulk and shear moduli of materials.

2.2.1. Bounds on the bulk and shear moduli. The hierarchy of scale-dependent bounds on the elastic response of random microstructures is shown by employing the spatial ergodicity, WSS properties and the variational principles of continuum elasticity as follows (see Ostoja-Starzewski [18], Kanit et al. [29], Sab [30], Huet [31])

$$\langle \mathbf{S}_1^t \rangle^{-1} \leq \dots \leq \langle \mathbf{S}_{\delta'}^t \rangle^{-1} \leq \langle \mathbf{S}_\delta^t \rangle^{-1} \leq \dots \leq \mathbf{C}_\infty^{eff} \dots \leq \langle \mathbf{C}_\delta^d \rangle \leq \langle \mathbf{C}_{\delta'}^d \rangle \dots \leq \langle \mathbf{C}_1^d \rangle \quad \forall \delta' \leq \delta. \quad (2.17)$$

By using Eq. (2.17), the hierarchy of bounds on the bulk and shear moduli for isotropic stiffness tensors can be seen as follows (see Ranganathan and Ostoja-Starzewski [10] and Ostoja-Starzewski et al. [23])

$$K^R \leq \dots \leq \langle K_{\delta'}^t \rangle \leq \langle K_\delta^t \rangle \leq \dots \leq K_\infty^{eff} \dots \leq \langle K_\delta^d \rangle \leq \langle K_{\delta'}^d \rangle \dots \leq K^V \quad \forall \delta' \leq \delta, \quad (2.18a)$$

$$G^R \leq \dots \leq \langle G_{\delta'}^t \rangle \leq \langle G_\delta^t \rangle \leq \dots \leq G_\infty^{eff} \dots \leq \langle G_\delta^d \rangle \leq \langle G_{\delta'}^d \rangle \dots \leq G^V \quad \forall \delta' \leq \delta, \quad (2.18b)$$

where V is the Voigt bound and R is the Reuss bound defined as follows (see Hill [32])

$$K^V = \frac{(C_{11} + C_{22} + C_{33}) + 2(C_{12} + C_{23} + C_{31})}{9}, \quad (2.19)$$

$$K^R = \frac{1}{(S_{11} + S_{22} + S_{33}) + 2(S_{12} + S_{23} + S_{31})}, \quad (2.20)$$

$$G^V = \frac{(C_{11} + C_{22} + C_{33}) - (C_{12} + C_{23} + C_{31}) + 3(C_{44} + C_{55} + C_{66})}{15}, \quad (2.21)$$

$$G^R = \frac{15}{4(S_{11} + S_{22} + S_{33}) - 4(S_{12} + S_{23} + S_{31}) + 3(S_{44} + S_{55} + S_{66})}. \quad (2.22)$$

In the subsequent section, we illustrate the methodology for obtaining rigorous bounds

on the bulk and shear moduli of random materials.

2.2.2. Homogenization methodology. The methodology for obtaining scale-dependent bounds on the elastic response of polycrystals is schematically shown in Fig. (1). These microstructures were created using Voronoi tessellation which is a set of 3D entities (zones of influence of a specific set of points which relates to their centres) that completes the 3D space without gaps or overlaps (see Quey et al. [33]). From a physical perspective, a Voronoi tessellation represents a process of solidification in which all grains form at the same time and isotropically grow at the same rate. The software Neper was used for generating the polycrystals using Voronoi tessellation which has been widely employed in several applications including elastic wave propagation [34], fracture [35], magnetism [36], geology [37], fatigue [38] and plasticity [39]. In Neper, the tessellation module (-T) was used to create the morphology and the seeds of the cells were randomly distributed in the microstructure. The weights associated to the seeds were then assigned using a Dirac distribution and a standard tessellation was implemented in order to ensure that all seeds were located inside the domain. Subsequently, a structured mesh was created using hexahedral elements and the element size was specified through the element characteristic length. Next, an input file was generated using Neper and an example for generating a polycrystal with 5000 grains can be seen in Fig. (2). This input file was then imported to Abaqus in order to assign material properties and boundary conditions (Dirichlet and Neumann). It has to be noted that the single crystal has a reference stiffness tensor with independent components depending upon the crystal class (from cubic to triclinic). Therefore, the reference tensor was rotated in order to assign the material property for each individual crystal in the polycrystal by using a set of uniformly generated rotation tensors. This procedure was carried out using Matlab where the required number of realizations were also generated. A batch file was run using Python for solving the boundary value problems in Abaqus. By

performing ensemble averaging in Matlab, the bounds on the aggregate response were obtained. The software R was then used for generating the plots and this procedure was repeated for all grain sizes.

In the next chapter, we consider the scale-dependent response of single phase polycrystals with individual grains belonging to any crystal class. In doing so, we introduce the notion of an elastic scaling function and determine its specific form through numerical simulations.

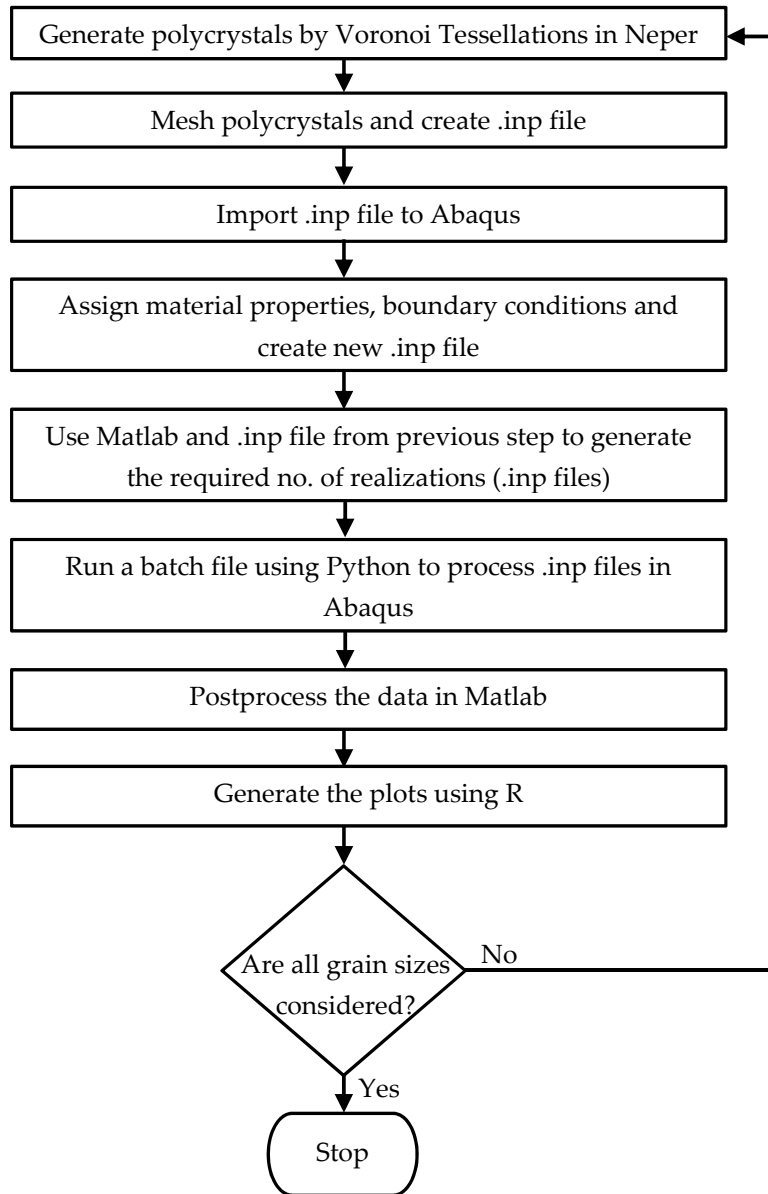


Figure 1. Methodology Flowchart

```

ridwan@Ridwan-Linux:~$ neper -T -n 5000 -id 1 -domain 'cube(1,1,1)' -format tess -weight 'dirac(0.02)' -ttype 'standard' -o Tess5000dirac

ridwan@Ridwan-Linux:~$ neper -M Tess5000dirac.tess -eltype 'hex' -o 5000dirac -format 'inp' -cl 1/35 -order 2

ridwan@Ridwan-Linux:~$ neper -V Tess5000dirac.tess -datacellcol id -print Tess5000dir
  
```

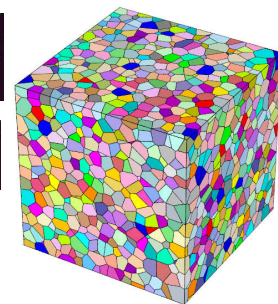


Figure 2. Generating a Polycrystal in Neper

Chapter 3

Scaling Laws in Elastic Polycrystals With Individual Grains Belonging to Any Crystal Class

In this chapter, we develop unifying scaling laws describing the response of elastic polycrystals at finite mesoscales. These polycrystals are made up of individual grains belonging to any crystal class (from cubic to triclinic) and are generated by Voronoi tessellations with varying grain sizes. Rigorous scale-dependent bounds are then obtained by setting up and solving Dirichlet and Neumann boundary value problems consistent with the Hill-Mandel homogenization condition. The results generated are benchmarked with existing numerical results in special cases and the effect of grain shape on the scaling behavior is investigated. The convergence to the effective elastic properties with increasing number of grains is established by analyzing 5180 boundary value problems. This leads to the notion of an elastic scaling function which takes a power-law form in terms of the Universal Anisotropy Index and the mesoscale. Based on the scaling function, a material scaling diagram is constructed using which the convergence to the effective properties can be analyzed for any elastic microstructure¹.

3.1 Introduction

Composite materials are widely used nowadays due to the dire need for novel materials with unique properties. With the advent of additive manufacturing, composites can be designed with superior structural integrity (enhanced fracture toughness [3]) and 3D printed with controlled variation of material properties [41, 42]. Such properties are dependent upon the structure of the composite (proportions of each component, shape of the particles and arrangement of the particles) and

¹See also [40] M. R. Murshed and S. I. Ranganathan, “Scaling laws in elastic polycrystals with individual grains belonging to any crystal class,” *Acta Mechanica*, vol. 228, no. 4, pp. 1525 – 1539, 2017. [Online]. Available: <http://dx.doi.org/10.1007/s00707-016-1774-3>

the corresponding property of each individual component in a composite (electrical, thermal and mechanical property). Thus, the structure-property relationship is a fundamental aspect in the design of composite materials which comprises of polycrystalline aggregates. These polycrystals are a collection of single crystals (grains) that have arbitrary orientations. The properties of polycrystalline aggregates depend upon the length scale and the single crystal orientation. By randomly assigning each crystal orientation in a polycrystal, one can obtain the effective isotropic response. In the context of elasticity, the effective property (shear and bulk moduli) can be estimated corresponding to a Representative Volume Element (RVE).

However, determining the appropriate size of the RVE in order to accurately obtain the aggregate response is still a challenge in composite material theory. Therefore, various homogenization techniques have been developed in order to estimate the effective property. One such approach is the Mori-Tanaka method which relates the average stress in an inclusion to the average stress in the matrix for obtaining the aggregate response in polycrystals (see Sevostianov and Kachanov [43]). However, the Mori-Tanaka's scheme may violate the Hashin-Shtrikman bounds for multiphase composites as well as yield a non-symmetric stiffness tensor and thereby the effective response cannot be obtained. An alternate method based on Maxwell's scheme for estimating the effective property of anisotropic multiphase composites was proposed by Sevostianov [44]. In that study, the author modified Maxwell's scheme by taking into account the shape of the inclusion and illustrated that an ellipsoidal shape captured the effective response accurately. On the contrary, selecting an inappropriate shape of the inclusion will cause the stiffness and compliance tensors to lose positive definiteness and the effective property cannot be determined.

An alternate approach to quantify the size of RVE, free of any positive

definiteness violation, is to implement the Hill-Mandel homogenization condition [7, 8] and obtain rigorous bounds as solutions to scale-dependent stochastic boundary value problems (Dirichlet and Neumann). This homogenization technique has attracted a great deal of interest over the past few decades within the context of elasticity [9, 10, 19, 21, 45], thermal conductivity [11, 12, 46, 47], electrical conductivity [13], thermoelasticity [14, 15, 48], flow in porous media [16, 17, 49], fracture and damage phenomena in random microstructures [18] and nonlinear elastic and inelastic materials [50, 51, 52, 53]. This framework has been employed by several other authors including Kanit et al. [29] and El Houdaigui et al. [54] for estimating the size of RVE. In particular, Kanit et al. [29] investigated three-dimensional Voronoi mosaic-shaped linearly elastic materials in order to determine the effective properties of two-phase heterogeneous microstructures at specific length scales. In their work, the authors showed the minimum number of realizations required for a given RVE size by taking into account the following: i) physical property of the material; ii) material contrast; iii) volume fraction of individual phases; iv) relative precision for estimating the effective property. In addition, the authors observed that for a specific precision and number of realizations, one can obtain the minimal size of the RVE in order to determine the effective response. Along similar lines, El Houdaigui et al. [54] analyzed three-dimensional Voronoi mosaic as polycrystalline morphology in order to determine the number of grains (N_G) required in a RVE for estimating the effective elastic properties of Copper. The authors used a variety of boundary conditions (Dirichlet and Neumann) and obtained the mean shear modulus as a function of N_G . It was seen that the minimum number of grains required is related to the evolution of the standard deviation of the effective property (shear modulus).

Several other authors have employed the framework of stochastic micromechanics in order to demonstrate the concept of a scaling function through the convergence of Dirichlet and Neumann bounds. In particular, Ranganathan

and Ostoja-Starzewski [19] obtained the scale-dependent bounds on the aggregate response of elastic random polycrystals at finite length scales. Subsequently, scaling laws were established that takes into account the mesoscale along with the universal anisotropy measure of single crystals. By employing the elastic scaling function, a material scaling diagram was constructed to quantify the size of the RVE for multifarious random polycrystals. Along similar lines, Dalaq et al. [55] illustrated the scale-dependence of thermal conductivities in two-phase planar random checkerboards at all length scales. In their study, the authors analyzed microstructures with 50% volume fractions with a variety of material combinations. It was observed that the scaling function depends upon the material contrast and the mesoscale. Subsequently, a material scaling diagram was generated which estimates the size of the RVE for any combination of individual phases.

Similarly, Raghavan et al. [13] examined the scale-dependent electrical conductivity of two-phase random microstructures at arbitrary volume fractions and material contrasts. In particular, the authors demonstrated the convergence of the mesoscale bounds to the effective electrical properties with increasing length scales. Also, the authors derived the scaling function which takes into account the volume fraction, phase contrast and mesoscale. It was seen that the size of the RVE can be estimated using a material scaling diagram for a range of composite microstructures. More recently, Zhang and Ostoja-Starzewski [56] analyzed the frequency-dependent scaling function for linear viscoelastic materials. In their work, the authors numerically simulated planar random checkerboard microstructures that had volume fractions of 50% at two-phases (elastic and viscoelastic), varying mesoscales ($\delta = 2,4,8,16$) and frequencies (0.05 Hz - 50 Hz). Next, the hierarchies of mesoscale bounds on shear and bulk type responses were obtained and a scaling function was developed in order to capture the scaling trend to RVE. It was observed that the scaling function is dependent upon the frequency and the mesoscale.

In summary, a significant amount of literature exists regarding the homogenization of random composites in order to determine the effective properties. However, to the best of our knowledge there is no framework to unify the scaling behavior of elastic polycrystals belonging to any crystal class. In the current work, we establish unifying scaling laws at finite mesoscales describing the elastic response of random polycrystals. These polycrystals are generated by Voronoi tessellations with varying grain sizes including 25, 400, 1000 and 5000 grains. The materials studied are Cu, Zn, SnF₂, S, An₉₆, Zr, α Ti and Fe₂O₃ as these belong to various crystal classes (from cubic to triclinic). Subsequently, rigorous bounds are obtained at finite length scales as solutions to stochastic boundary value problems (Dirichlet and Neumann) based on the Hill-Mandel homogenization condition. The results generated are benchmarked with existing numerical solutions for Cu. Also, the effect of grain shape (Voronoi tessellations and Cubic-shaped geometry) on the scaling behavior of cubic crystals (Lithium) is demonstrated. By analyzing 5180 boundary value problems, we illustrate that the scale-dependent bounds on the elastic response of polycrystals converge to the effective properties with increasing number of grains. In doing so, we generalize the notion of an elastic scaling function which depends upon the Universal Anisotropy Index and the number of grains in the domain. Finally, the scaling function is employed to develop the material scaling diagram that can be used to precisely estimate the size of the RVE.

3.2 Elastic Scaling Function

Consider the form of scaling function which is postulated in chapter 2 (see section 2.2). For single phase materials, the functional form can be defined as follows

$$\langle \mathbf{C}_\delta^d \rangle :: \langle \mathbf{S}_\delta^t \rangle = \lim_{\delta \rightarrow \infty} \langle \mathbf{C}_\delta^d \rangle :: \langle \mathbf{S}_\delta^t \rangle + f(C^{ij}, \delta), \quad (3.1a)$$

$$f(C^{ij}, \delta) = f(C^{ij}, A^U, \delta), \quad (3.1b)$$

where $f(C^{ij}, A^U, \delta)$ is the dimensionless elastic scaling function and A^U is the Universal Anisotropy Index that was first introduced by Ranganathan and Ostoja-Starzewski [22]. Unlike the scaling function first proposed by Ranganathan and Ostoja-Starzewski [19] that was restricted to crystals with cubic symmetry, the function in Eq. (3.1a) is applicable to all crystal classes. The variable C^{ij} represents all the single crystal elastic constants depending on the crystal class as given below

i) Cubic

$$C^{ij} \equiv (C_{11}, C_{12}, C_{44}), \quad (3.2a)$$

ii) Hexagonal

$$C^{ij} \equiv (C_{11}, C_{12}, C_{13}, C_{33}, C_{44}), \quad (3.2b)$$

iii) Tetragonal

$$C^{ij} \equiv (C_{11}, C_{12}, C_{13}, C_{33}, C_{44}, C_{66}), \quad (3.2c)$$

iv) Trigonal

$$C^{ij} \equiv (C_{11}, C_{12}, C_{13}, C_{14}, C_{33}, C_{44}), \quad (3.2d)$$

iv) Orthorhombic

$$C^{ij} \equiv (C_{11}, C_{12}, C_{13}, C_{22}, C_{23}, C_{33}, C_{44}, C_{55}, C_{66}), \quad (3.2e)$$

v) Monoclinic

$$C^{ij} \equiv (C_{11}, C_{12}, C_{13}, C_{15}, C_{22}, C_{23}, C_{25}, C_{33}, C_{35}, C_{44}, C_{46}, C_{55}, C_{66}), \quad (3.2f)$$

vi) Triclinic

$$C^{ij} \equiv (C_{11}, C_{12}, C_{13}, C_{14}, C_{15}, C_{16}, C_{22}, C_{23}, C_{24}, C_{25}, C_{26}, \\ C_{33}, C_{34}, C_{35}, C_{36}, C_{44}, C_{45}, C_{46}, C_{55}, C_{56}, C_{66}). \quad (3.2g)$$

Substituting Eqs. (2.15) and (3.1a) into Eq. (2.14) gives the functional form of the elastic scaling function as

$$f(C^{ij}, A^U, \delta) = 5 \frac{\langle G_\delta^d \rangle}{\langle G_\delta^t \rangle} + \frac{\langle K_\delta^d \rangle}{\langle K_\delta^t \rangle} - 6. \quad (3.3)$$

The boundary value problems listed under Eqs. (2.7a) and (2.7b) in chapter 2 can be solved numerically in order to obtain the right hand side of Eq. (3.3). We now discuss the homogenization methodology for single phase polycrystals using Fig. (3). The grain sizes ($N_G = 25, 400, 1000$ and 5000) that are taken into consideration are based on the work by El Houdaigui et al. [54]. Using Eqs. (2.7a) and (2.7b), Dirichlet and Neumann type boundary value problems (5180) are solved and upon ensemble averaging, the bounds on the elastic response are obtained. In the next section, we illustrate the properties and bounds on the scaling function.

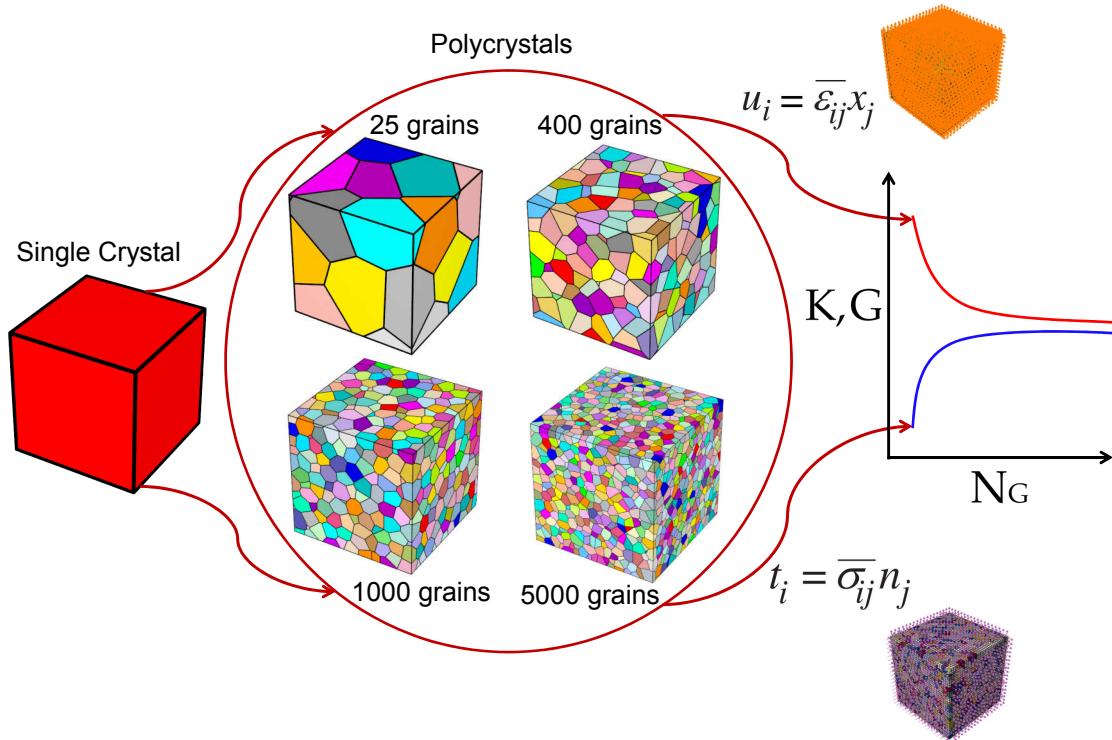


Figure 3. Homogenization methodology for single phase elastic polycrystals

3.2.1. Properties and bounds on the elastic scaling function. The elastic scaling function $f(C^{ij}, A^U, \delta)$ which is postulated in Eq. (3.1a) has the following properties

$$f(C^{ij}, A^U, \delta \approx \infty) = 0, \quad (3.4)$$

where the scaling function is equal to zero when the mesoscale is infinite. Also, when the single crystals are locally isotropic ($A^U = 0$), the scaling function is equal to zero

$$f(C^{ij}, A^U = 0, \delta) = 0. \quad (3.5)$$

In addition, the bounds on the elastic scaling function can be seen as follows

$$f(C^{ij}, A^U, \delta \approx \infty) \leq f(C^{ij}, A^U, \delta) \leq f(C^{ij}, A^U, \delta = 1) \quad \forall 1 \leq \delta \leq \infty. \quad (3.6)$$

By employing Eqs. (3.4) and (3.3) in (3.6), the following bounds are obtained

$$0 \leq f(C^{ij}, A^U, \delta) \leq A^U = 5 \frac{G^V}{G^R} + \frac{K^V}{K^R} - 6 \quad \forall 1 \leq \delta \leq \infty. \quad (3.7)$$

It has to be noted that if C^{ij} is changed to αC^{ij} (α is a real number), the scaling function remains the same

$$f(\alpha C^{ij}, A^U, \delta) = f(C^{ij}, A^U, \delta). \quad (3.8)$$

It is therefore possible to postulate the various forms of the scaling function once the parameters of f are identified.

3.3 Results and Discussion

Let us now consider rigorous bounds on the elastic properties of random polycrystals at finite length scales. These polycrystals are generated numerically

according to spatially ergodic and WSS properties. Also, the polycrystals are white-noise random fields as these have no spatial correlations. In the subsequent sections, we validate our numerical results for the shear modulus of Cu with the results published in the literature by El Houdaigui et al. [54]. After validating the numerical model, the effect of grain shape (Voronoi tessellations and Cubic-shaped geometry) on the scaling function is analyzed. Then, eight materials (see Table 1) across all crystal classes (from cubic to triclinic) are studied and 5180 numerical simulations are performed in order to illustrate the scale-dependent bounds on the aggregate response. In doing so, Dirichlet and Neumann boundary conditions are imposed on polycrystals with varying grain sizes (25, 400, 1000 and 5000) as follows:

1) Dirichlet problem:

i) For extracting shear modulus: $\varepsilon_{11}^0 = \varepsilon_{22}^0 = 0.05$, $\varepsilon_{33}^0 = -0.1$, $\varepsilon_{12}^0 = \varepsilon_{13}^0 = \varepsilon_{23}^0 = 0$;

ii) For extracting bulk modulus: $\varepsilon_{11}^0 = \varepsilon_{22}^0 = \varepsilon_{33}^0 = 0.05$, $\varepsilon_{12}^0 = \varepsilon_{13}^0 = \varepsilon_{23}^0 = 0$;

2) Neumann problem:

iii) For extracting shear modulus:

$\sigma_{11}^0 = \sigma_{22}^0 = 16$ GPa, $\sigma_{33}^0 = -32$ GPa, $\sigma_{12}^0 = \sigma_{13}^0 = \sigma_{23}^0 = 0$;

iv) For extracting bulk modulus: $\sigma_{11}^0 = \sigma_{22}^0 = \sigma_{33}^0 = 16$ GPa, $\sigma_{12}^0 = \sigma_{13}^0 = \sigma_{23}^0 = 0$.

Next, we proceed to develop a suitable form of the scaling function and construct the material scaling diagram for quantifying the size of RVE.

3.3.1. Benchmark results. We discuss the benchmarking studies that were performed in order to validate the results for Cu with the ones published in the literature by El Houdaigui et al. [54]. For Dirichlet boundary value problems, computational results showed that scale-dependent bounds converged to effective property (shear modulus) as percentage difference is less than 2% for all grain sizes (see Table 2). Similarly, for Neumann boundary value problems, numerical results indicated that bounds approached effective property as percentage difference is less

than 4% for all grains sizes (see Table 3). In the subsequent section, the effect of grain shape on scaling behavior of random microstructures is illustrated.

Table 1

Materials analyzed across all crystal classes

Crystal Class	Material	G^V (GPa)	G^R (GPa)	K^V (GPa)	K^R (GPa)	A^U
Cubic	Cu ^a	54.63	40.03	137.07	137.07	1.82
Hexagonal	Zn ^b	44.82	34.13	75.08	61.58	1.79
Monoclinic	SnF ₂ ^c	13.80	10.30	17.90	16.50	1.78
Orthorhombic	S ^d	7.22	6.17	20.60	17.56	1.03
Triclinic	An ₉₆ ^e	42.45	35.70	88.74	84.10	0.99
Tetragonal	Zr ^f	21.70	18.40	21.00	19.00	1.00
Hexagonal	α Ti ^g	44.20	42.59	105.00	105.00	0.19
Trigonal	Fe ₂ O ₃ ^h	94.70	91.90	98.30	97.20	0.16

^a El Houdaigui et al. [54]; ^b Berryman [57]; ^c Watt [58]; ^d Lide [59]; ^e Brown et al. [60]; ^f Watt and Peselnick [61]; ^g Ledbetter and Kim [62]; ^h Berryman [57]

Table 2

Model validation for shear modulus (GPa) of Cu (Dirichlet)

No. of Grains	No. of Realizations	Current Work	El Houdaigui et al. [54]	% difference
25	100	51.77	52.54	1.48
400	50	50.03	50.09	0.12
1000	25	49.94	49.79	0.31
5000	10	49.48	49.34	0.29

Table 3

Model validation for shear modulus (GPa) of Cu (Neumann)

No. of Grains	No. of Realizations	Current Work	El Houdaigui et al. [54]	% difference
25	100	44.90	43.40	3.47
400	50	47.15	47.31	0.34
1000	25	47.49	47.57	0.15
5000	10	48.17	48.39	0.46

3.3.2. Effect of grain shape on scaling function and size of RVE.

The effect of the grain shape on the scaling behavior of Lithium is now discussed as its Universal Anisotropy Index is very high ($A^U = 8.43$). In addition, we have selected the grain sizes (8, 27, 64 and 512) based on the work by Ranganathan and Ostoja-Starzewski [19] (see Fig. 4a). Fig. (4b) illustrates the scale-dependent bounds on the shear modulus for grains generated by Voronoi tessellations and Cubic-shaped grains. It can be seen that as $N_G \rightarrow \infty$ ($\delta \rightarrow \infty$), there is no significant difference in the results obtained using the geometry generated by Voronoi tessellations and the Cubic-shaped geometry. This is consistent with the observations of Ranganathan and Ostoja-Starzewski [19] and Bhattacharya and Suquet [63]. In fact, the scaling and rescaled functions are almost identical except for $N_G = 8$ (see Fig. 4c & d). Therefore, we conclude that it does not matter whether Voronoi or Cubic-shaped geometry is used in order to quantify the size of RVE. Also, if the A^U is significantly large, the shape of the grains is not important for homogenizing the aggregate response. In addition, the RVE size is not affected by the grain shape when $A^U = 0$. Next, we proceed to demonstrate the scale-dependent bounds of all the materials analyzed across the various crystal classes.

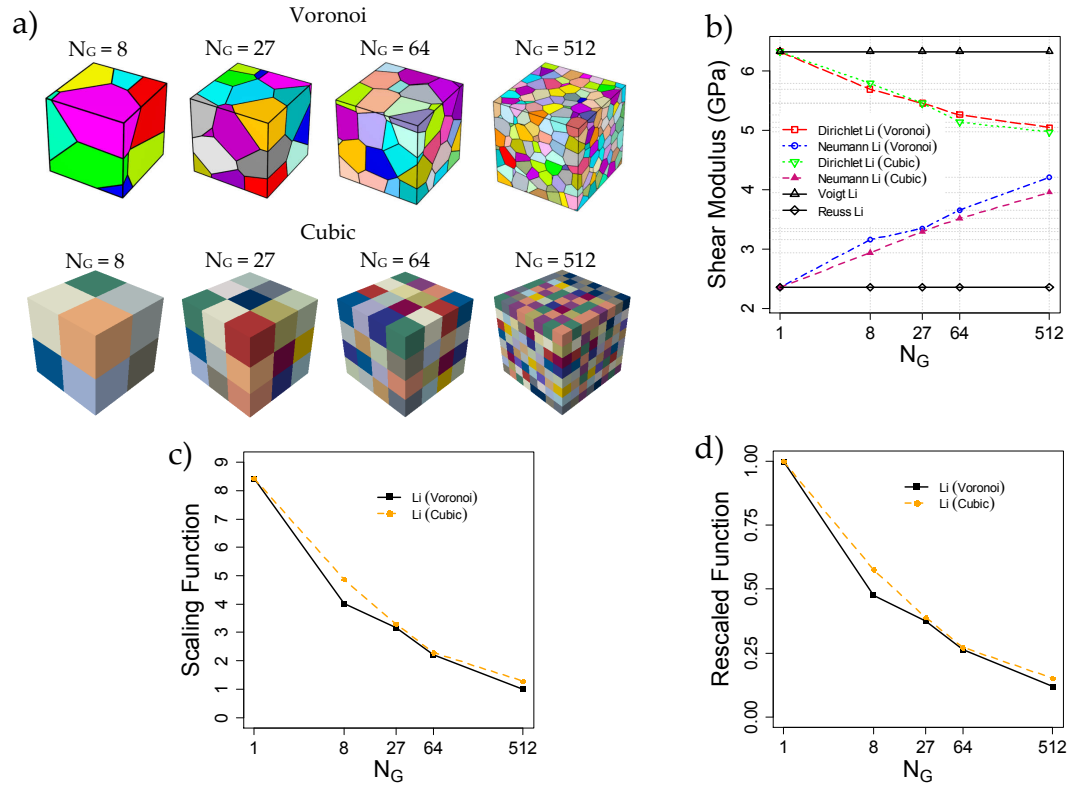


Figure 4. Comparison of grain shapes for Lithium: a) Voronoi and Cubic-shaped geometry b) Scale-dependent bounds for shear modulus c) Scaling Function d) Rescaled Function

3.3.3. Bounds on the aggregate response. Following the methodology in section 2.2.2., we now numerically obtain scale-dependent bounds on all the materials. The upper and lower bounds correspond to the Voigt and Reuss estimates. The scale-dependent bounds of the shear modulus for Cu as well as the bounds for the shear and bulk moduli for Zn and SnF₂ can be observed in Fig. (5). It is evident that the bounds converge to the effective property with an increase in the number of grains from 25 to 5000 (see Fig. 5). Along similar lines, the scale-dependent bounds of S, An₉₆ and Zr get tighter as the number of grains increase (see Fig. 6). Similarly, the elastic response of α Ti and Fe₂O₃ indicate that the bounds approach the effective property (shear and bulk moduli) as the grain size increases (see Fig. 7).

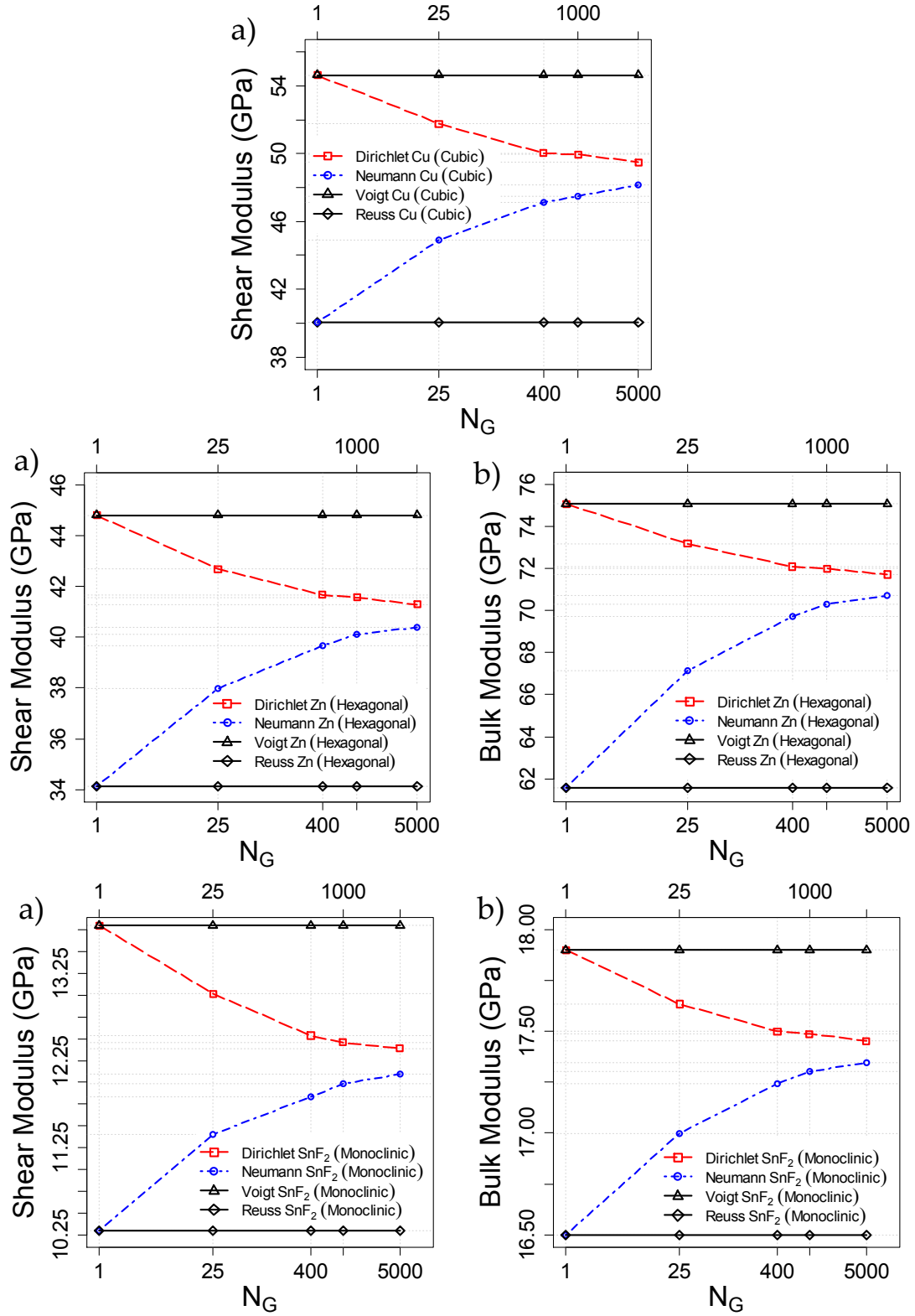


Figure 5. Bounds on elastic moduli of Cu (top), Zn (center) & SnF₂ (bottom): a) shear modulus b) bulk modulus

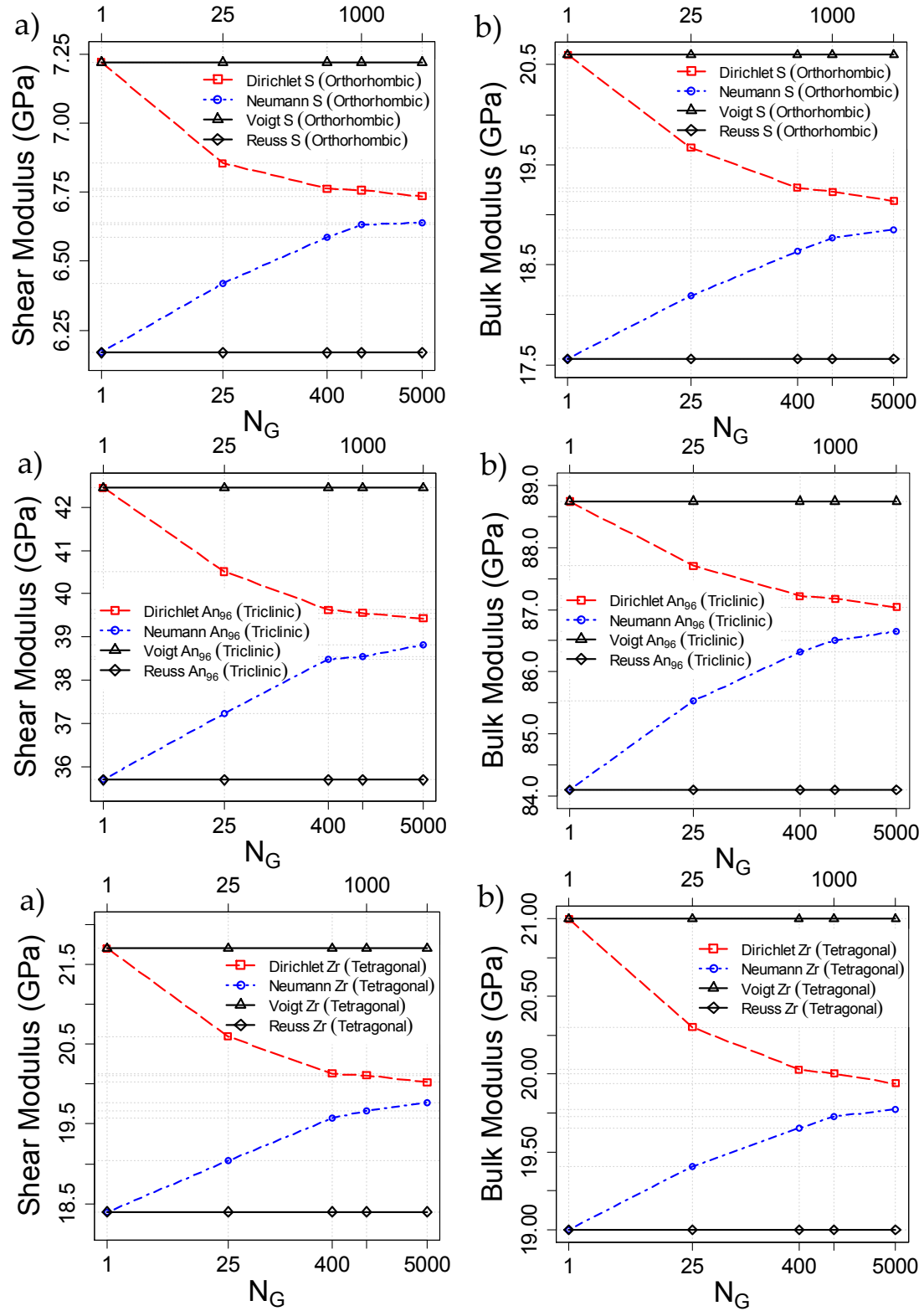


Figure 6. Bounds on elastic moduli of S (top), An₉₆ (center) & Zr (bottom): a) shear modulus b) bulk modulus

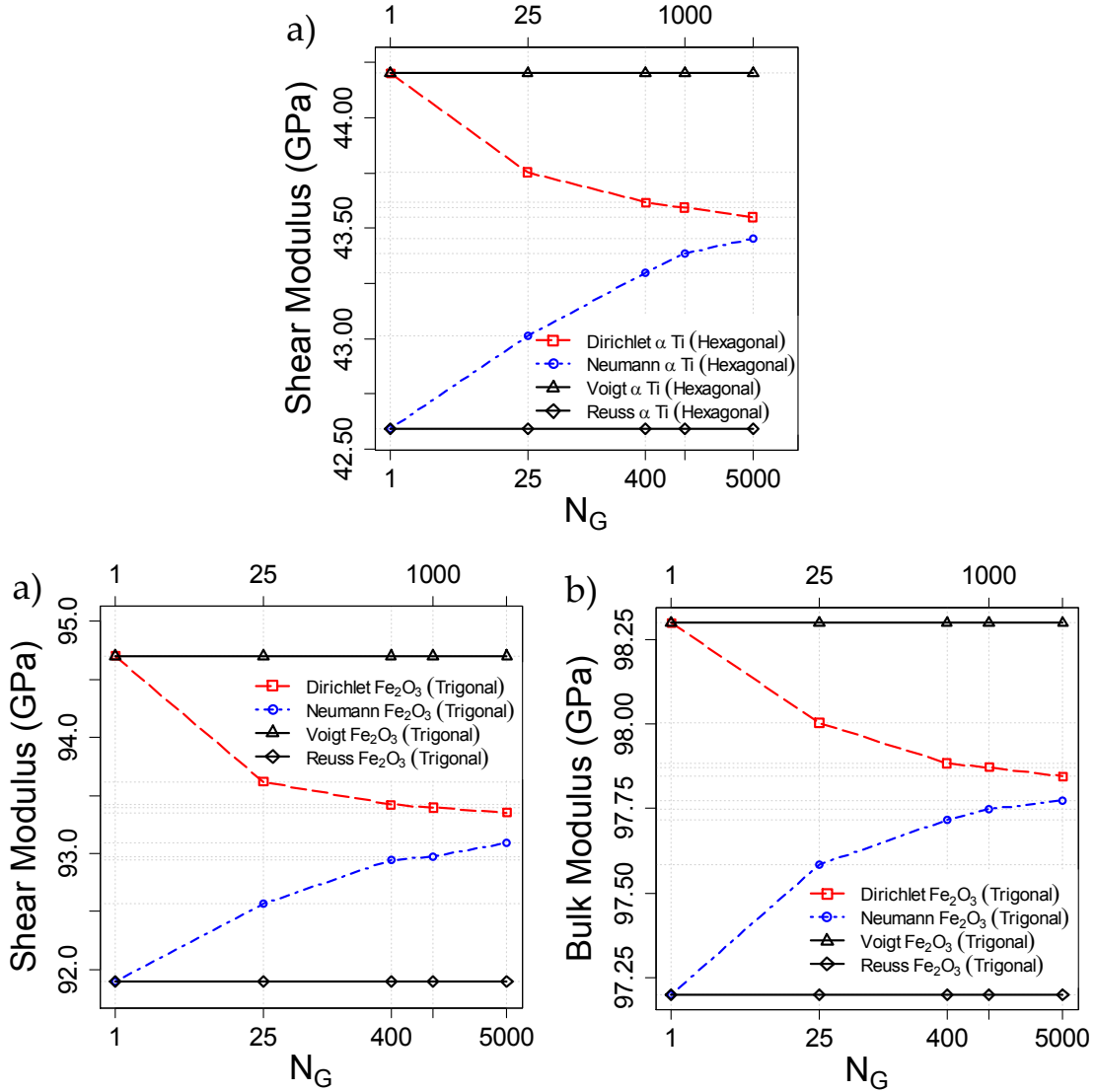


Figure 7. Bounds on elastic moduli of α Ti (top) & Fe_2O_3 (bottom): a) shear modulus b) bulk modulus

Let us now discuss the scaling behavior of all the materials studied. The Universal Anisotropy Index, A^U , for Cu, Zn and SnF_2 are almost identical (see Table 1) and therefore they will be analyzed together. Fig. (8) shows that the scaling functions for these materials are quite close to one another and it is reasonable to state that the scaling function depends only on the A^U and the mesoscale, δ . Therefore, we rewrite Eq. (3.3) as follows

$$f(C^{ij}, A^U, \delta) \equiv f(A^U, \delta). \quad (3.9)$$

The scaling functions for S, An₉₆ and Zr can be seen in Fig. (8). Once again, the scaling functions for these three materials are very close to each other. A similar phenomenon is observed for α Ti and Fe₂O₃ as the scaling functions for these two materials are almost identical (see Fig. 8).

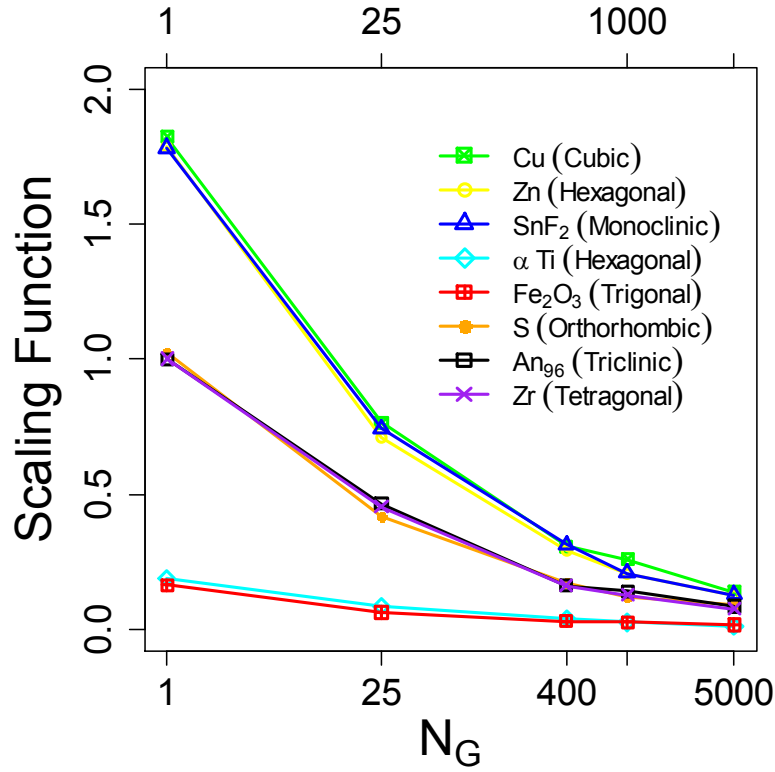


Figure 8. Scaling Function for single phase materials

3.4 Constructing the Scaling Function

The functional form of the scaling function is illustrated by rewriting Eq. (3.7) as follows

$$0 \leq \frac{1}{A^U} f(A^U, \delta) \leq 1. \quad (3.10)$$

It is very interesting to observe that the rescaled function defined in Eq. (3.10) is identical for all the materials belonging to any crystal class as seen in Fig. (9). The

slight scatter in the results plotted in Fig. (9) can be attributed to the finite number of realizations used to obtain the ensemble averages. Therefore, it is reasonable to state that the rescaled function, f^* , is independent of the Universal Anisotropy Index, A^U , and is only a function of the mesoscale, δ . By redefining the scaling function, it can be seen that

$$f(A^U, \delta) = A^U f^*(\delta), \quad (3.11)$$

where $f^*(\delta)$ is the material-independent rescaled function.

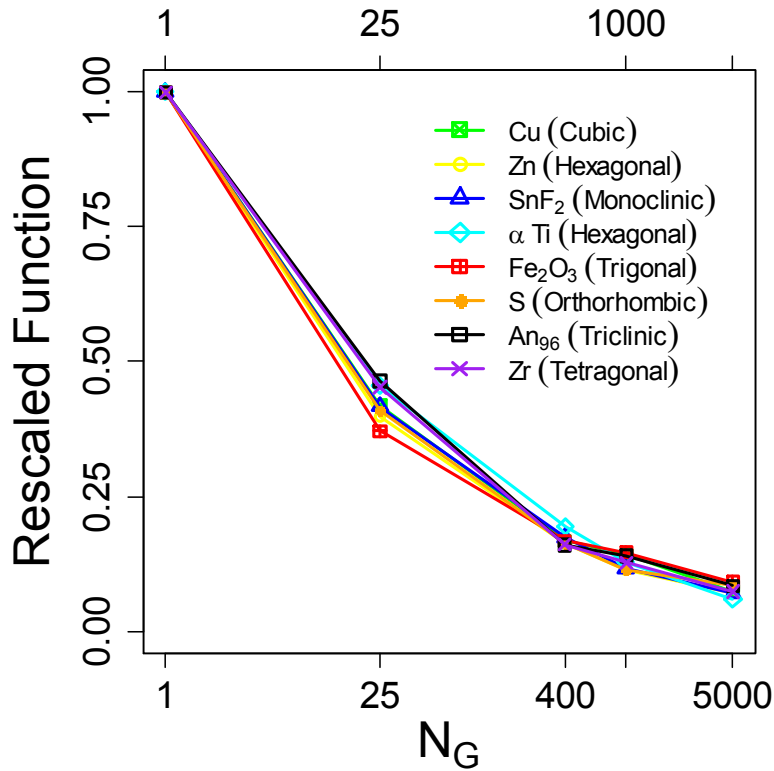


Figure 9. Rescaled Scaling Function for single phase materials

Next, the mean values of $f^*(\delta)$ in Fig. (9) are taken in order to construct the effective averaged rescaled function (obtained through numerical simulations) and curve fit it (see Fig. 10). Based on the effective function and its fit, $f^*(\delta)$ takes the following form

$$f^*(\delta) = (\delta)^{-0.89}. \quad (3.12)$$

At this stage, it is convenient to illustrate the scaling function using Eqs. (3.11) and (3.12) as follows

$$f(A^U, \delta) = A^U (\delta)^{-0.89}, \quad \delta = (N_G)^{\frac{1}{3}}. \quad (3.13)$$

This form of the scaling function takes into account all the properties defined in section 3.2.1. By employing Eq. (3.13), we reconstruct the scaling function for all the materials as shown in Fig. (11). It is clear from this plot that this formulation captures the scaling function accurately and unifies the treatment of a wide spectrum of materials across all crystal classes (from cubic to triclinic).

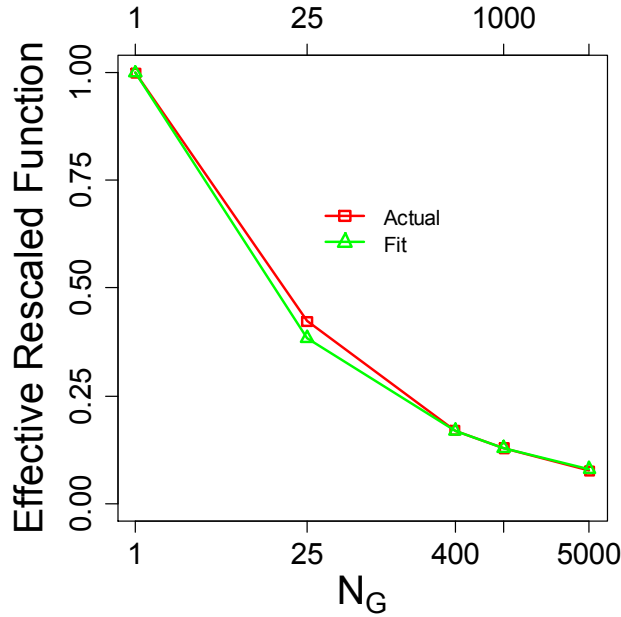


Figure 10. Effective Rescaled Scaling Function & Fit for single phase materials

3.5 Material Scaling Diagram

The contours of scaling function in (A^U, N_G) space based on Eq. (3.13) can be seen in Fig. (12). For any finite value of scaling function within the range $(0.01 \leq f \leq 0.23)$, the number of grains (N_G) required to homogenize the effective response

can be obtained using Fig. (12). Also, it is observed that the curves shift towards higher number of grains and vice-versa as the scaling function decreases. It has to be noted that the value of scaling function determines the appropriate size of RVE. Theoretically, when number of grains is infinite, scaling function becomes zero or when $A^U = 0$ (crystal is locally isotropic). For practical purposes, one can choose a finite value of scaling function in order to determine the number of grains required for homogenization. This concept is illustrated by choosing a specific value of scaling function ($f = 0.2$) and constructing Fig. (13) based on this value for a variety of elastic random polycrystals. For a material with low anisotropy (Fe_2O_3), RVE is approached at $N_G = 1$ ($\delta = 1$). Finally, for a material with high anisotropy (Cu), number of grains required for homogenization is $N_G = 1678$ ($\delta \cong 12$).

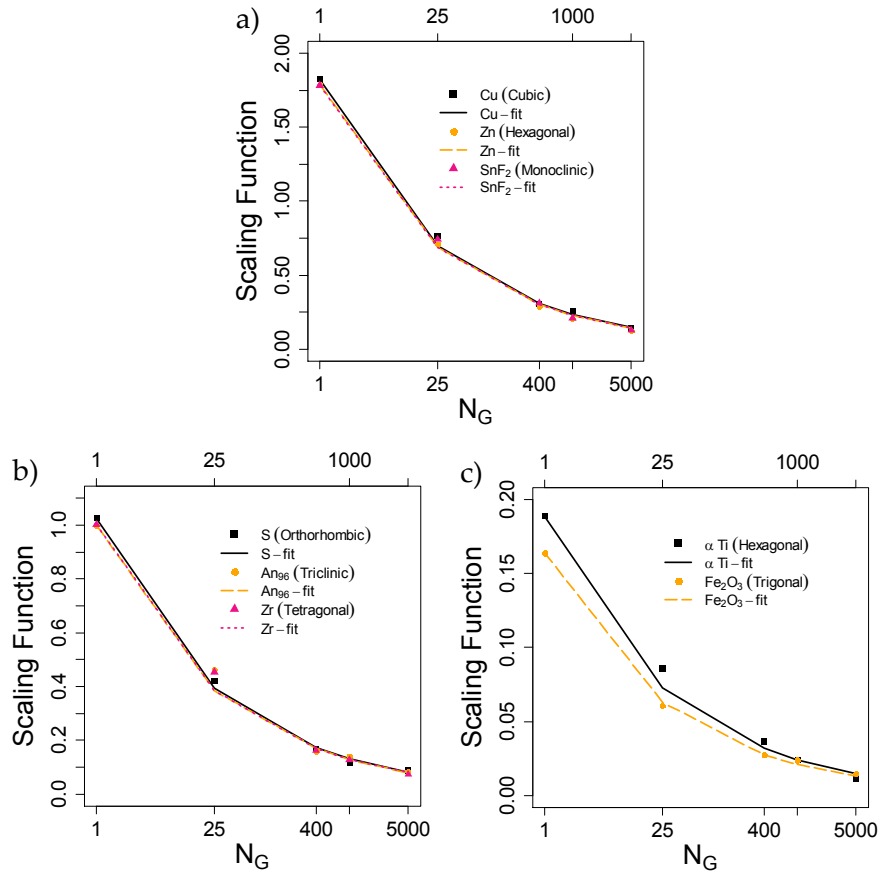


Figure 11. Scaling Function & Fit for single phase materials: a) Cu, Zn, SnF₂ b) S, An₉₆, Zr c) α Ti, Fe₂O₃

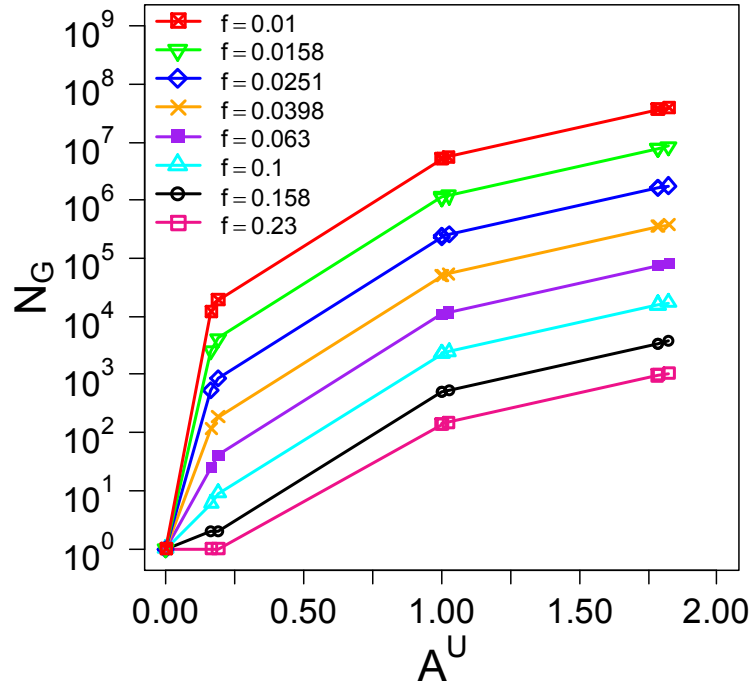


Figure 12. Contours of Scaling Function for $0.01 \leq f \leq 0.23$

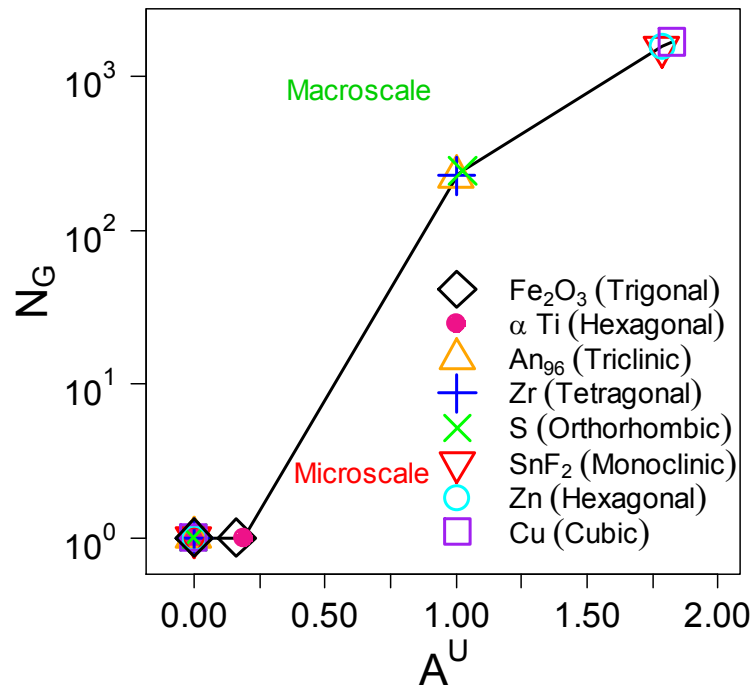


Figure 13. Material Scaling Diagram at $f = 0.2$ (single phase materials)

3.6 Summary

In chapter 3, we have demonstrated the methodology to obtain scale-dependent bounds on the elastic response of polycrystals by solving stochastic boundary value problems (Dirichlet and Neumann) consistent with the Hill-Mandel homogenization condition. In doing so, we established a framework to unify the treatment of a variety of elastic random polycrystals across all crystal classes (from cubic to triclinic) in terms of the elastic scaling function. This specific form of the scaling function takes into account the Universal Anisotropy Index, A^U , and the number of grains in the domain. In addition, some characteristics of the scaling function were shown such as the scaling function is zero at infinite grain sizes or when the crystals are locally isotropic ($A^U = 0$). Subsequently, a material scaling diagram was constructed that allows us to estimate the number of grains required for homogenization. To the best of our knowledge, this is the first attempt to unify the scaling behavior for single phase elastic random polycrystals belonging to any crystal class. In the subsequent chapter, we consider a case study of highly anisotropic single crystals belonging to lower symmetry class. Subsequently, rigorous bounds are obtained on the elastic response of these microstructures and the results are compared with all other methods that are widely available in the literature.

Chapter 4

Case Study: Hill-Mandel Condition and Bounds on Lower Symmetry Elastic Crystals

Despite advances in contemporary micromechanics, there is a void in the literature on a versatile method for estimating the effective properties of polycrystals comprising of highly anisotropic single crystals belonging to lower symmetry class. Basing on variational principles in elasticity and the Hill-Mandel homogenization condition, we illustrate a versatile methodology to fill this void. It is demonstrated that the bounds obtained using the Hill-Mandel condition are tighter than the Voigt and Reuss bounds, the Hashin-Shtrikman bounds as well as a recently proposed self-consistent estimate by Kube and Arguelles even for polycrystals with highly anisotropic single crystals².

4.1 Introduction

Polycrystalline materials are widely used in engineering applications as the need to develop new materials with unique properties has significantly increased (enhanced fracture toughness [3], high thermal conductivity [4], superior electrical conductivity [5]). These microstructures consist of collection of single crystals with random orientations and individual grains belonging to any crystal class (from cubic to triclinic). When these crystals are oriented randomly, collectively they exhibit an effective elastic behavior that is isotropic upon ensemble averaging. However, despite advances in contemporary micromechanics over the past several decades, it is still a challenge to predict the effective properties of such polycrystals especially when the single crystals are highly anisotropic and have lower elastic symmetry (see [19, 10, 65]).

²See also [64] M. R. Murshed and S. I. Ranganathan, "Hill-Mandel condition and bounds on lower symmetry elastic crystals," *Mechanics Research Communications*, vol. 81, pp. 7 – 10, 2017. [Online]. Available: <https://doi.org/10.1016/j.mechrescom.2017.01.005>

In the past, several techniques have been used to predict the elastic response of materials and some of these are noteworthy. Voigt [66] developed the upper bound on the elastic moduli by assuming uniform strain throughout the material. Along similar lines, Reuss [67] obtained the lower bound on the aggregate response by considering uniform stress in the composite. It was later demonstrated by Hashin-Shtrikman [68] using variational principles that the upper and lower bounds for the elastic moduli of polycrystals can be tighter than the Voigt and Reuss bounds. Also, the authors applied their approach to a two-phase alloy that had cubic symmetry and illustrated that the theoretical results were in good agreement with the experimental results. Several other authors had employed Hashin-Shtrikman's variational principles method for polycrystals from various crystal classes. In particular, Watt and Peselnick [61] demonstrated explicit expressions for the bounds on the elastic moduli of polycrystalline aggregates composed of hexagonal, trigonal and tetragonal crystals. Also, the authors showed that Hashin-Shtrikman bounds were within the Voigt and Reuss bounds. Similarly, Berryman [57] developed analytical formulas in order to obtain self-consistent estimates for the shear and bulk moduli of random polycrystals with hexagonal, trigonal and tetragonal symmetries. In addition, the author was successful in obtaining the self-consistent estimates within the Hashin-Shtrikman bounds for all the crystal classes considered in that study.

An alternate approach for estimating the effective property is the Mori-Tanaka method which relates the average stress in an inclusion to the average stress in the matrix in multiphase composites. In particular, Norris [69] investigated two-phase composites and proved that the elastic moduli obtained using Mori-Tanaka method always satisfied the Hashin-Shtrikman bounds. Also, for spherical particles, it was demonstrated that the results for the effective moduli of multiphase composites were within the Hashin-Shtrikman bounds.

While several theories exist in the literature for determining the elastic response of materials, somewhat tighter bounds for elastic constants have only been recently obtained for microstructures with lower symmetry. In particular, Brown [70] illustrated a numerical technique for obtaining the Hashin-Shtrikman bounds for materials belonging to any crystal class. In that study, the author estimated the Hashin-Shtrikman bounds as a function of the properties of a reference isotropic material and reported the results for crystals with triclinic symmetry. Following Brown's [70] computational procedure, Kube and Arguelles [65] developed theoretical expressions for obtaining the self-consistent estimates of polycrystals and illustrated an iterative approach to solve these expressions. It was seen that the estimates can be obtained for a variety of geological materials that have monoclinic and triclinic symmetries.

In this study, we illustrate an alternate method for obtaining tighter bounds than Kube and Arguelles [65] using the Hill-Mandel homogenization condition (see Hill [7] and Mandel [8]). In the subsequent sections, we establish scale-dependent bounds on the elastic response of random polycrystals with 10000 grains which were generated using Voronoi tessellations. By analyzing stochastic boundary value problems (Dirichlet and Neumann) consistent with the Hill-Mandel condition, we illustrate that the aggregate response of polycrystals converge to the effective properties. Subsequently, tighter bounds are obtained than the bounds and self-consistent estimates published in the literature by Voigt-Reuss [66, 67], Hashin-Shtrikman [68] and Kube and Arguelles [65].

4.2 Methodology

The microstructure of a polycrystal with 10000 grains can be seen in Fig. (14a) along with the Dirichlet (see Fig. 14b) and Neumann (see Fig. 14c) boundary conditions. These polycrystals are generated by Voronoi tessellations using the

software Neper (see Quey et al. [33]). Subsequently, Dirichlet and Neumann boundary value problems are solved [using Eqs. (2.7a) and (2.7b) from chapter 2] and rigorous bounds are obtained on the elastic response of random microstructures. In the next section, we illustrate the bounds obtained using the Hill-Mandel homogenization condition and compare the results with the bounds and self-consistent estimates published in the literature by Voigt-Reuss [66, 67], Hashin-Shtrikman [68] and Kube and Arguelles [65].

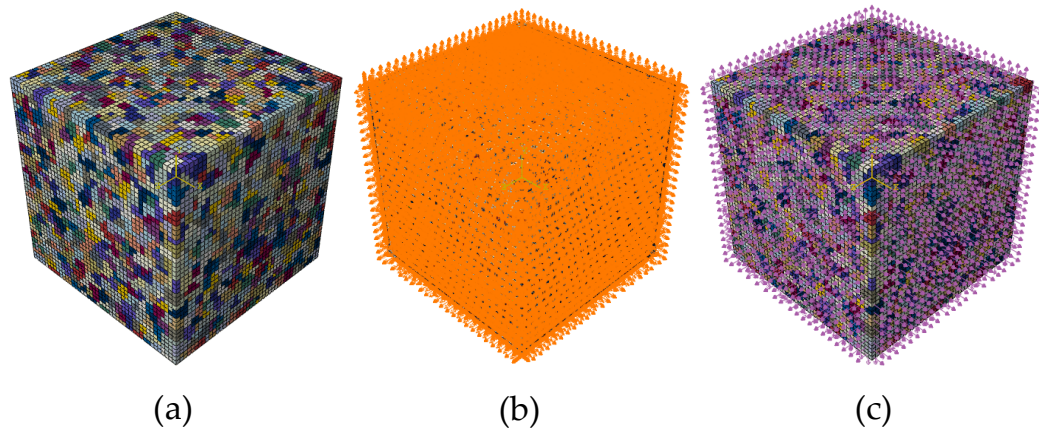


Figure 14. A 10000-grain Voronoi tessellation: (a) Microstructure of a Polycrystal with 10000 grains (b) Microstructure subjected to Dirichlet Boundary Condition (c) Microstructure subjected to Neumann Boundary Condition

4.3 Results and Discussion

TABLES-4 and 5 summarize the results obtained on several lower symmetry elastic crystals with increasing single crystal anisotropy. The Dirichlet (d) and Neumann (t) bounds obtained using the Hill-Mandel condition are compared with the Voigt and Reuss bounds [66, 67], the Hashin-Shtrikman bounds [68] as well as the more recent self-consistent (SC) estimate proposed by Kube and Arguelles [65]. It is evident that all estimates are within Voigt and Reuss bounds. Also, it can be noted that Hashin-Shtrikman bounds are tighter than Voigt and Reuss bounds. It is evident that the bounds obtained using the Hill-Mandel condition are even tighter

than the Hashin-Shtrikman bounds. Although, the recently proposed self-consistent (SC) estimate is always between the Hashin-Shtrikman bounds, it does not fall within the bounds obtained using the Hill-Mandel condition. It is interesting to note that the self-consistent estimate proposed by Kube and Arguelles [65] is very close to the lower bound obtained using the Hill-Mandel condition (use of uniform traction boundary conditions).

Table 4

Bounds & self-consistent estimates (SC) of shear (μ) moduli (GPa): Bounds include Voigt(V)-Reuss(R), Hashin-Shtrikman(HS) & Dirichlet(d) - Neumann(t)

Material	A^U	μ^R	μ^-HS	μ^t	μ^{SC}	μ^d	μ^+HS	μ^V
1	1.00	35.70	38.20	38.95	38.90	39.33	39.70	42.50
2	1.80	10.30	11.60	12.12	12.10	12.39	12.40	13.80
3	2.80	6.20	7.00	7.13	7.10	7.31	7.70	9.10
4	3.60	4.20	4.90	5.44	5.40	5.59	5.80	6.90
5	4.50	11.50	14.00	15.17	15.00	15.73	16.90	20.10

Materials: 1) An_{96} (triclinic); 2) Tin Difluoride (monoclinic); 3) Ethylene diamine tartrate (monoclinic); 4) Oxalic Acid dihydrate (monoclinic); 5) Lithium hydrogen oxalate monohydrate (triclinic)

Table 5

Bounds & self-consistent estimates (SC) of bulk (κ) moduli (GPa): Bounds include Voigt(V)-Reuss(R), Hashin-Shtrikman(HS) & Dirichlet(d) - Neumann(t)

Material	A^U	κ^R	κ^-HS	κ^t	κ^{SC}	κ^d	κ^+HS	κ^V
1	1.00	84.10	86.20	86.71	86.70	87.01	87.20	88.70
2	1.80	16.50	17.10	17.36	17.30	17.44	17.50	17.90
3	2.80	15.90	19.20	19.63	19.50	20.27	21.30	24.50
4	3.60	10.80	11.90	12.46	12.40	12.70	13.00	14.30
5	4.50	22.10	27.50	29.83	29.70	31.11	33.20	39.30

Materials: 1) An_{96} (triclinic); 2) Tin Difluoride (monoclinic); 3) Ethylene diamine tartrate (monoclinic); 4) Oxalic Acid dihydrate (monoclinic); 5) Lithium hydrogen oxalate monohydrate (triclinic)

In view of variational principles in elasticity, any estimate for the effective property must lie within the Voigt and Reuss bounds, Hashin-Shtrikman bounds and the bounds obtained using the Hill-Mandel condition [19]. Clearly, the self-consistent estimate does not satisfy this hierarchy of bounds and this is even more evident as the single crystal anisotropy increases. For instance, consider Lithium hydrogen oxalate monohydrate from TABLE-6, it is seen that the self-consistent estimate can be up to 5 % higher than the upper bound using the Hill-Mandel condition.

Table 6

Comparison of results using Hill-Mandel condition with self-consistent estimates for shear and bulk moduli (GPa)

Material	A^U	$\frac{\mu^{SC}-\mu^t}{\mu^{SC}} \times 100$	$\frac{\mu^{SC}-\mu^d}{\mu^{SC}} \times 100$	$\frac{\kappa^{SC}-\kappa^t}{\kappa^{SC}} \times 100$	$\frac{\kappa^{SC}-\kappa^d}{\kappa^{SC}} \times 100$
1	1.00	-0.13	-1.10	-0.01	-0.36
2	1.80	-0.15	-2.38	-0.33	-0.81
3	2.80	-0.47	-2.91	-0.64	-3.93
4	3.60	-0.82	-3.58	-0.44	-2.44
5	4.50	-1.14	-4.84	-0.44	-4.75

Materials: 1) An_96 (triclinic); 2) Tin Difluoride (monoclinic); 3) Ethylene diamine tartrate (monoclinic); 4) Oxalic Acid dihydrate (monoclinic); 5) Lithium hydrogen oxalate monohydrate (triclinic)

4.4 Summary

We have proposed a methodology based on Hill-Mandel condition using which, tighter bounds were obtained on elastic polycrystals (monoclinic and triclinic materials) when compared to all the existing methods proposed in the literature. The methodology is very versatile and is based on variational principles in elasticity. Also, the bounds obtained can be made even tighter by considering polycrystals with more number of grains (greater than 10,000) for numerical simulations. So far, we focused on obtaining scale-dependent bounds on single phase polycrystals. In the subsequent chapter, we introduce the notion of ‘Heterogeneous Anisotropy Index’ and examine its role on the finite-size scaling of two-phase random polycrystals.

Chapter 5

Heterogeneous Anisotropy Index and Scaling in Two-Phase Random Polycrystals

Under consideration is the finite-size scaling of the elastic properties in two-phase random polycrystals with individual grains belonging to any arbitrary crystal class. These polycrystals are generated by Voronoi tessellations with varying grain sizes and volume fractions. Any given realization of such a microstructure sampled randomly is highly anisotropic and heterogeneous. Using extremum principles in elasticity, we introduce the notion of a ‘Heterogeneous Anisotropy Index (A_H^U)’ and examine its role in the scaling of elastic properties at finite mesoscales (δ). The relationship between A_H^U and the Universal Anisotropy Index, A^U [22] is established for special cases. The scale-dependent bounds are then obtained by setting up and solving 9250 Dirichlet and Neumann type boundary value problems consistent with the Hill-Mandel homogenization condition. Subsequently, the concept of an elastic scaling function is introduced that takes a power-law form in terms of A_H^U and δ . Finally, a material scaling diagram is constructed by employing the elastic scaling function which captures the convergence to the effective properties for any two-phase elastic microstructure³

5.1 Introduction

Polycrystalline materials have unique properties and are commonly used in several engineering applications (such as elasticity [23], heat conduction [50], fracture [35], magnetism [36]). In particular, two-phase polycrystalline materials have been used in minerals engineering [37], thermal conductivity [72], plasticity [73]. Such materials have grains belonging to any crystal class (from cubic to

³See also [71] S. I. Ranganathan, M. R. Murshed and L. Costa, “Heterogeneous anisotropy index and scaling in two-phase random polycrystals,” *under minor revision*, 2017.

triclinic) with arbitrary orientations. These microstructures are highly anisotropic and heterogeneous at finite scales, thereby posing a challenge to the predictive modeling of their collective behavior. The objective of this research is to introduce the notion of a ‘Heterogeneous Anisotropy Index’ and examine its role in the finite-size scaling of two-phase random polycrystals.

In the past, several authors have investigated the effective response of two-phase materials and some of these are noteworthy. In particular, Hashin-Shtrikman [74] used variational principles to illustrate upper and lower bounds on elastic moduli of two-phase materials. In their study, the authors analyzed a two-phase alloy (Tungsten Carbide) and proved that their theoretical results were in good agreement with experimental results. Along similar lines, Walpole [75] examined upper and lower bounds as well as self-consistent estimates on the elastic moduli of materials. The author developed theoretical expressions for shear and bulk moduli of composites with transversely isotropic inclusions (needle or disc shape) at random orientations and arbitrary volume fractions. Similarly, Watt et al. [76] analyzed bounds on shear and bulk moduli of several two-phase composites with different volume fractions ($v_f = 0, 0.2, 0.4, 0.8, 1$). It was demonstrated that the effective moduli of these materials were within Hashin-Shtrikman bounds for all volume fractions.

An alternate approach to determine the effective properties is to employ the Mori-Tanaka method (see Mori and Tanaka [77]) that relates the average stress in an inclusion to the average stress in the matrix in multiphase composites. Benveniste [78] analyzed two-phase materials with anisotropic elastic constituents by reformulating the Mori-Tanaka method in order to determine the aggregate response. In the study, the author illustrated that shear and bulk moduli for two-phase composites were within Hashin-Shtrikman bounds. Along similar lines, Weng [79] analyzed the

relationship between Hashin-Shtrikman-Walpole (H-S-W) bounds and Mori-Tanaka (M-T) method for composites. The author investigated multiphase materials with unidirectionally aligned constituents and observed the following: i) For spherical inclusions, M-T moduli will always fall within H-S-W bounds when the matrix is neither the softest nor the hardest phase; ii) For circular fibers, M-T method will lie within the H-S-W bounds like the spherical case; iii) For thin discs, M-T moduli will be an exact solution like the H-S-W bounds (upper and lower bounds coincide as these are independent of the material property).

More recently, Ni and Chiang [80] predicted the effective elastic constants of two-phase isotropic materials. In their work, the authors used phase-field microelasticity (PFM) that is based on Eshelby's effective eigenstrain approach (see Eshelby [81]) in order to obtain the elastic properties at specific volume fractions ($v_f = 0.1, 0.2, 0.3, 0.4, 0.5$). It was shown that PFM method can be employed only for lower volume fractions ($v_f < 0.2$) to estimate shear and bulk moduli.

An alternate method for studying the effective response of materials is to implement Hill-Mandel homogenization condition and obtain rigorous bounds as solutions to scale-dependent stochastic boundary value problems. In this approach, the microstructure should be spatially statistically homogeneous, ergodic and macroscopically uniform boundary conditions (Dirichlet and Neumann) are to be applied so that the effective response is independent of the boundary conditions. This methodology has been successfully employed by several authors within the context of elasticity [19, 10, 64], thermal conductivity [11, 46, 47], thermoelasticity [82, 14, 48, 15], flow in porous media [16, 17], fracture and damage phenomena in random microstructures [18] and nonlinear elastic and inelastic materials [51, 52]. This framework has been employed by several other authors in order to determine the effective response of two-phase polycrystals. In particular, Kanit et al. [29]

analyzed three-dimensional Voronoi mosaic shaped linearly elastic materials in order to determine the effective properties of two-phase microstructures. In their work, the authors used several boundary conditions (Dirichlet and Neumann) and obtained shear and bulk moduli of two-phase materials at a specific volume fraction ($v_f = 0.7$). The authors also observed that their elastic moduli were within Voigt-Reuss [66, 67] (upper bound and lower bound) as well as Hashin-Shtrikman bounds. Along similar lines, Kanit et al. [83] investigated real two-phase microstructures using a digital representation of their morphology and obtained the effective response. In their study, the authors analyzed 3D confocal images of polycrystalline ice and polymeric cream which were phase 1 and phase 2, respectively. Subsequently, the authors performed numerical simulations using Dirichlet and Neumann boundary conditions on two-phase microstructures and showed that shear and bulk moduli were within Voigt-Reuss as well as Hashin-Shtrikman bounds.

Several other authors have also employed the Hill-Mandel homogenization condition to demonstrate the concept of a scaling function. This function unifies the treatment of a wide variety of materials by describing the effective response of random polycrystals through the convergence of Dirichlet and Neumann bounds. Recently, the scaling function has been studied in 3D elasticity (for individual grains belonging to any crystal class from cubic to triclinic) [40] and previously in 3D heat conduction [12], 2D elasticity [9], 2D heat conduction [55], 2D electrical conductivity [13] and 2D viscoelasticity [56].

In the subsequent sections, we generate two-phase random polycrystals by Voronoi tessellations and the microstructures considered in this study have real world applications. For instance, Ni-Cd is used in batteries [84], Sn-Ag is used for soldering joints [85], Ni-Cr is employed for strain gauge applications [86] and Ni-Co is used as a corrosion resistant coating [87]. We then vary the grain sizes (25, 400, 1000,

5000 grains) at different volume fractions ($v_f = 0, 0.25, 0.5, 0.75, 1$) in order to obtain rigorous bounds at finite mesoscales as solutions to stochastic boundary value problems (Dirichlet and Neumann) consistent with the Hill-Mandel homogenization condition. By analyzing 9250 boundary value problems, it will be demonstrated that these bounds converge to the effective elastic properties with increasing number of grains. We also illustrate the notion of an elastic scaling function which depends upon ‘Heterogeneous Anisotropy Index’ and number of grains in the domain. By employing the scaling function, a material scaling diagram is constructed which can be used to estimate the number of grains required for homogenization.

5.2 Elastic Scaling Function

In this section, we formulate the elastic scaling function for two-phase polycrystals and derive its functional form. By employing a similar methodology as illustrated in chapter 2, we obtain the following

$$\langle \mathbf{C}_\delta^d \rangle :: \langle \mathbf{S}_\delta^t \rangle = \lim_{\delta \rightarrow \infty} \langle \mathbf{C}_\delta^d \rangle :: \langle \mathbf{S}_\delta^t \rangle + f(C_{(1)}^{ij}, C_{(2)}^{ij}, v_f, \delta), \quad (5.1)$$

where $f(C_{(1)}^{ij}, C_{(2)}^{ij}, v_f, \delta)$ is the non-dimensional elastic scaling function and v_f is the volume fraction of phase 1. Also, C^{ij} applies to both $C_{(1)}^{ij}$ (phase 1) and $C_{(2)}^{ij}$ (phase 2) and represents all single crystal elastic constants as shown in section 3.2. By substituting Eqs. (2.15) and (5.1) into Eq. (2.14), the functional form of the elastic scaling function can be defined as

$$f(C_{(1)}^{ij}, C_{(2)}^{ij}, v_f, \delta) = 5 \frac{\langle G_\delta^d \rangle}{\langle G_\delta^t \rangle} + \frac{\langle K_\delta^d \rangle}{\langle K_\delta^t \rangle} - 6. \quad (5.2)$$

The right hand side of Eq. (5.2) is obtained by setting up and solving stochastic boundary value problems consistent with the Hill-Mandel condition. Let us now discuss the homogenization methodology for two-phase polycrystals which can be

seen in Fig. (15). The software Neper was used to generate the polycrystals ($N_G = 25, 400, 1000, 5000$) where each grain has a random orientation. By solving Dirichlet and Neumann type boundary value problems, scale-dependent bounds on the shear and bulk moduli of these microstructures can be obtained. In the subsequent section, the properties and bounds on the scaling function is demonstrated.

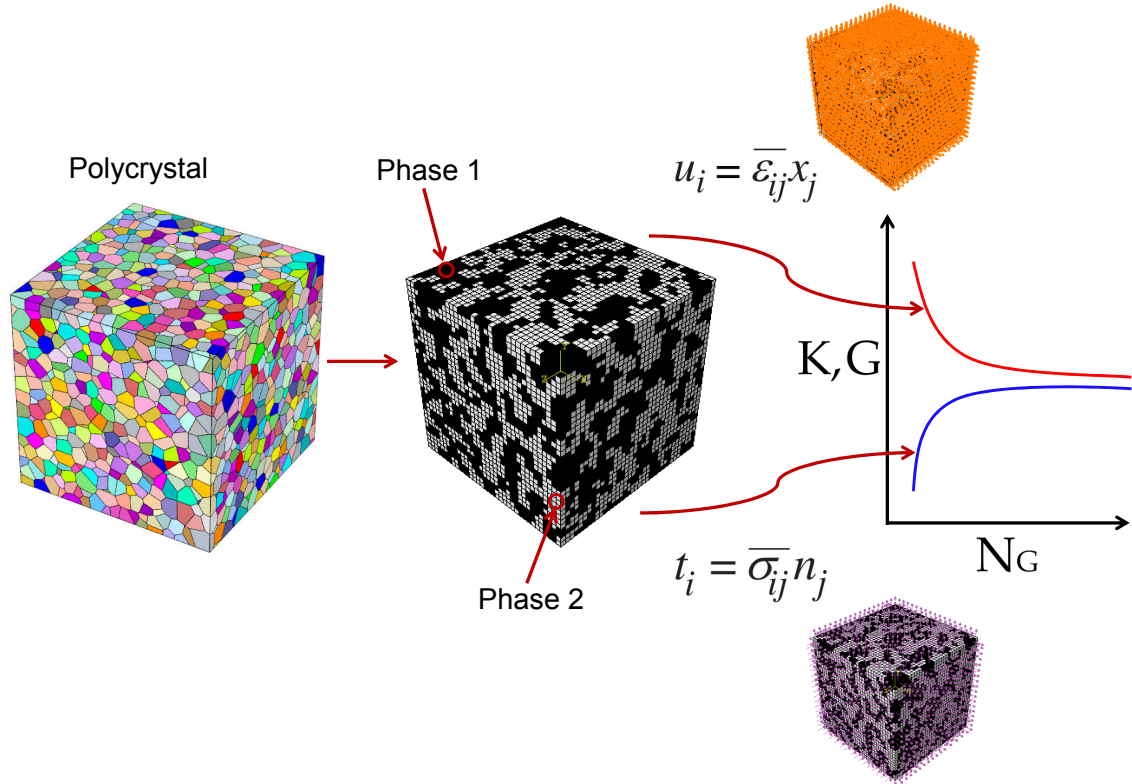


Figure 15. Homogenization methodology for two-phase elastic polycrystals

5.2.1. Properties and bounds on the elastic scaling function. The elastic scaling function $f(C_{(1)}^{ij}, C_{(2)}^{ij}, v_f, \delta)$ which is postulated in Eq. (5.1) has the following properties

$$f(C_{(1)}^{ij}, C_{(2)}^{ij}, v_f, \delta \approx \infty) = 0, \quad (5.3)$$

where the scaling function is equal to zero at infinite mesoscales. Also, if $C_{(1)}^{ij}$ and $C_{(2)}^{ij}$ are changed to $\alpha C_{(1)}^{ij}$ and $\alpha C_{(2)}^{ij}$ (α is a real number), the scaling function f

remains the same

$$f(\alpha C_{(1)}^{ij}, \alpha C_{(2)}^{ij}, v_f, \delta) = f(C_{(1)}^{ij}, C_{(2)}^{ij}, v_f, \delta). \quad (5.4)$$

Next, the bounds on the elastic scaling function can be seen as follows

$$\begin{aligned} f(C_{(1)}^{ij}, C_{(2)}^{ij}, v_f, \delta \approx \infty) &\leq f(C_{(1)}^{ij}, C_{(2)}^{ij}, v_f, \delta') \leq f(C_{(1)}^{ij}, C_{(2)}^{ij}, v_f, \delta) \\ &\dots \leq f(C_{(1)}^{ij}, C_{(2)}^{ij}, v_f, \delta = 1) \quad \forall 1 \leq \delta \leq \delta' \leq \infty. \end{aligned} \quad (5.5)$$

Several forms of the scaling function can now be postulated by identifying the appropriate parameters of f . In the subsequent section, the notion of ‘Heterogeneous Anisotropy Index’ is introduced that is a natural consequence of Eq. (5.5).

5.2.2. Heterogeneous Anisotropy Index. The ‘Heterogeneous Anisotropy Index’, A_H^U , which is obtained from Eq. (5.5) can be defined as follows

$$A_H^U = f(C_{(1)}^{ij}, C_{(2)}^{ij}, v_f, \delta = 1) \quad 0 \leq v_f \leq 1, \quad (5.6a)$$

$$\begin{aligned} A_H^U &= a + bv_f + cv_f^2, \\ a &= 5 \frac{G_{(2)}^V}{G_{(2)}^R} + \frac{K_{(2)}^V}{K_{(2)}^R} - 6, \\ b &= 5 \left[\frac{G_{(1)}^V}{G_{(2)}^R} + \frac{G_{(2)}^V}{G_{(1)}^R} - \frac{2G_{(2)}^V}{G_{(2)}^R} \right] + \frac{K_{(1)}^V}{K_{(2)}^R} + \frac{K_{(2)}^V}{K_{(1)}^R} - \frac{2K_{(2)}^V}{K_{(2)}^R}, \\ c &= 5 \left[\frac{G_{(1)}^V}{G_{(1)}^R} - \frac{G_{(1)}^V}{G_{(2)}^R} - \frac{G_{(2)}^V}{G_{(1)}^R} + \frac{G_{(2)}^V}{G_{(2)}^R} \right] + \frac{K_{(1)}^V}{K_{(1)}^R} - \frac{K_{(1)}^V}{K_{(2)}^R} - \frac{K_{(2)}^V}{K_{(1)}^R} + \frac{K_{(2)}^V}{K_{(2)}^R}, \end{aligned} \quad (5.6b)$$

and subscripts (1) and (2) represents phase 1 and phase 2, respectively. The index A_H^U turns out to be a function of 43 variables, 21 independent components for each phase and the volume fraction of either phase. It can also be seen that, when volume fraction of phase 1 is zero, we observe the following

$$f(C_{(1)}^{ij}, C_{(2)}^{ij}, v_f = 0, \delta = 1) = a = A_{(2)}^U \geq 0, \quad (5.7)$$

where $A_{(2)}^U$ is anisotropy of phase 2 only (single phase) and can be represented by Universal Anisotropy Index, A^U , of this phase (see Ranganathan and Ostoja-Starzewski [22]). Similarly, when volume fraction of phase 1 is one, we obtain the following

$$f(C_{(1)}^{ij}, C_{(2)}^{ij}, v_f = 1, \delta = 1) = a + b + c = A_{(1)}^U \geq 0, \quad (5.8)$$

and $A_{(1)}^U$ is anisotropy of phase 1 which is again a single phase material. Let us now discuss Fig. (16) which illustrates ‘Heterogeneous Anisotropy Index’ of 4 two-phase materials (Ni-Cd, Sn-Ag, Ni-Cr, Ni-Co) at different volume fractions.

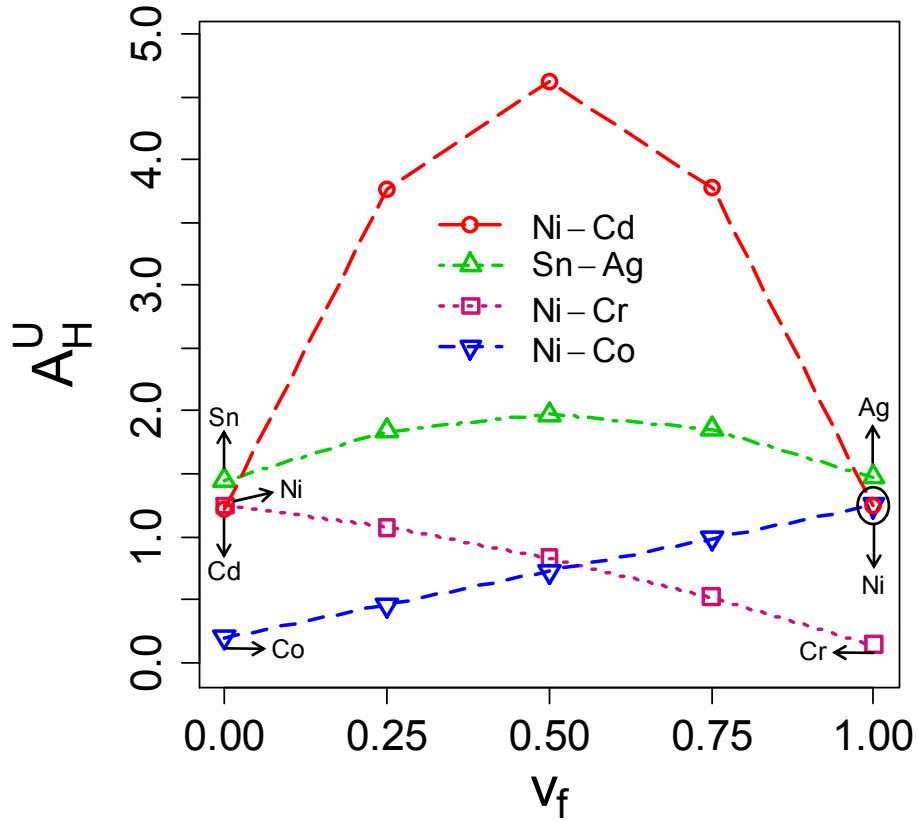


Figure 16. Heterogeneous Anisotropy Index (A_H^U) vs. Volume Fraction (v_f) for two-phase materials (Ni-Cd, Sn-Ag, Ni-Cr, Ni-Co)

We observe for Ni-Cd that A_H^U is similar at $v_f = 0.25$ as well as $v_f = 0.75$ and therefore scaling behavior is expected to be same at these volume fractions (see Fig. 16). A similar phenomenon can be seen for Sn-Ag as A_H^U is identical at $v_f = 0.25$ and $v_f = 0.75$. For Ni-Cr, A_H^U decreases from $A_H^U = 1.25$ to $A_H^U = 0.14$ with an increase in volume fraction from $v_f = 0$ to $v_f = 1$ (see Fig. 16). An opposite trend can be observed in Fig. (16) for Ni-Co as A_H^U increases from $A_H^U = 0.2$ to $A_H^U = 1.25$ with an increase in volume fraction. In the next section, we will obtain mesoscale constitutive behavior of two-phase random polycrystals by obtaining scale-dependent bounds as solutions to Dirichlet and Neumann type boundary value problems.

5.3 Results and Discussion

Consider the rigorous bounds on elastic constants of two-phase random polycrystals at finite mesoscales. These polycrystals are white-noise random fields as these have no spatial correlations. Also, these microstructures are generated numerically according to spatially ergodic and WSS properties. In the subsequent sections, we study 4 two-phase materials at different volume fractions ($v_f = 0, 0.25, 0.5, 0.75, 1$) and perform 9250 numerical simulations in order to illustrate the scale-dependent bounds on the effective elastic response (shear and bulk moduli). In doing so, we impose the following loading conditions to solve stochastic boundary value problems

1) Dirichlet problem:

i) For extracting shear modulus: $\varepsilon_{11}^0 = \varepsilon_{22}^0 = 0.05$, $\varepsilon_{33}^0 = -0.1$, $\varepsilon_{12}^0 = \varepsilon_{13}^0 = \varepsilon_{23}^0 = 0$;

ii) For extracting bulk modulus: $\varepsilon_{11}^0 = \varepsilon_{22}^0 = \varepsilon_{33}^0 = 0.05$, $\varepsilon_{12}^0 = \varepsilon_{13}^0 = \varepsilon_{23}^0 = 0$;

2) Neumann problem:

iii) For extracting shear modulus:

$\sigma_{11}^0 = \sigma_{22}^0 = 16$ GPa, $\sigma_{33}^0 = -32$ GPa, $\sigma_{12}^0 = \sigma_{13}^0 = \sigma_{23}^0 = 0$;

iv) For extracting bulk modulus: $\sigma_{11}^0 = \sigma_{22}^0 = \sigma_{33}^0 = 16$ GPa, $\sigma_{12}^0 = \sigma_{13}^0 = \sigma_{23}^0 = 0$.

5.3.1. Bounds on the aggregate response.

We demonstrate scale-dependent bounds of two-phase materials which are obtained by solving stochastic boundary value problems (see Figs. 17 & 18). For all volume fractions, upper and lower bounds correspond to Voigt and Reuss estimates, respectively. Fig. (17) illustrates Dirichlet and Neumann bounds on shear and bulk moduli for Ni-Cd and Sn-Ag. We observe that these bounds approach the effective property as number of grains increase from 25 to 5000 at all volume fractions (see Fig. 17).

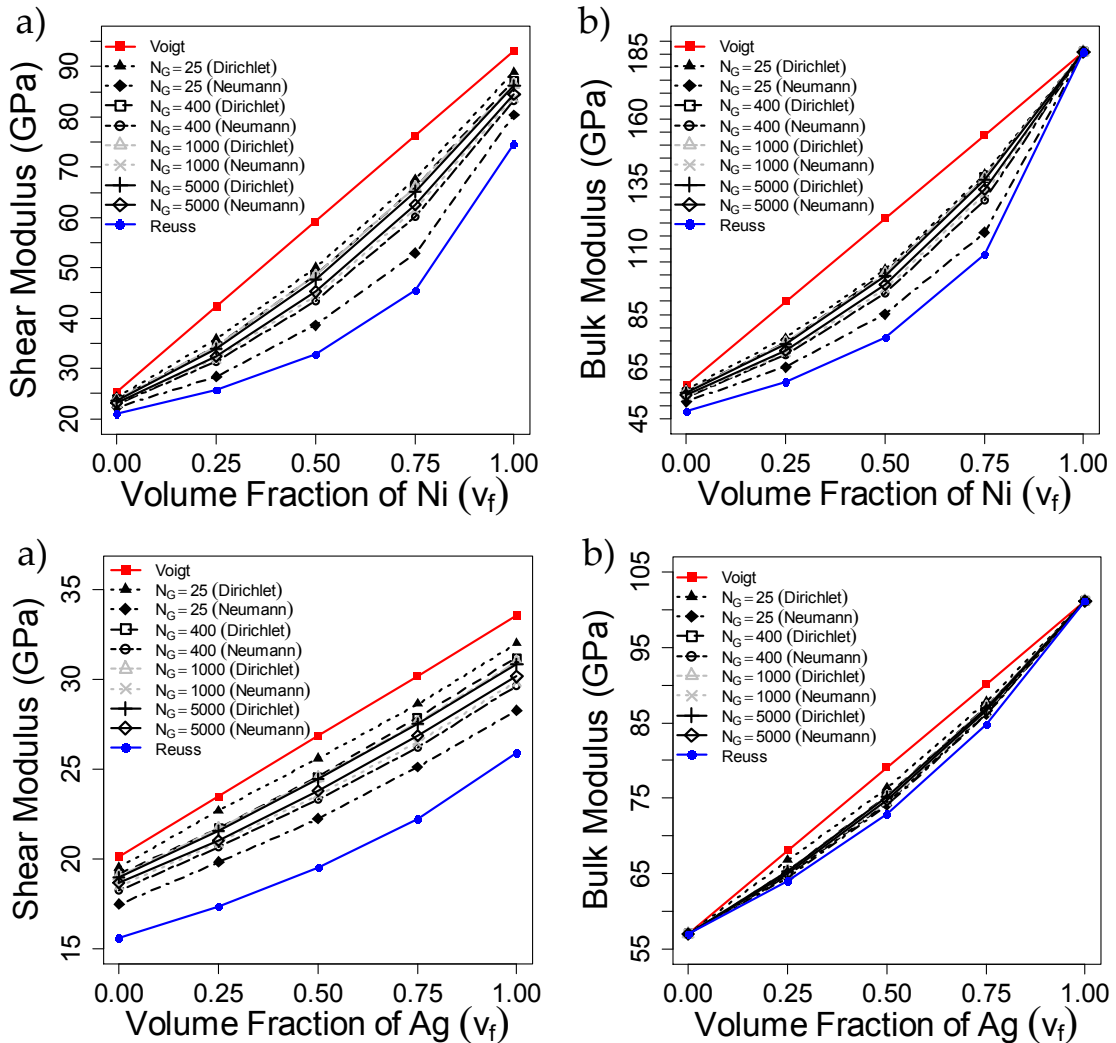


Figure 17. Bounds on elastic moduli of Ni-Cd (top) and Sn-Ag (bottom) at various volume fractions: a) shear modulus (GPa) b) bulk modulus (GPa)

Likewise, scale-dependent bounds on shear moduli of Ni-Cr and Ni-Co (see Fig. 18) converge to the aggregate response with an increase in number of grains. In addition, the bounds on bulk moduli for Ni-Cr are Voigt and Reuss estimates as Ni and Cr are cubic crystals. Along similar lines, upper and lower bounds on bulk moduli for Ni-Co correspond to the Voigt and Reuss averages (see Fig. 18).

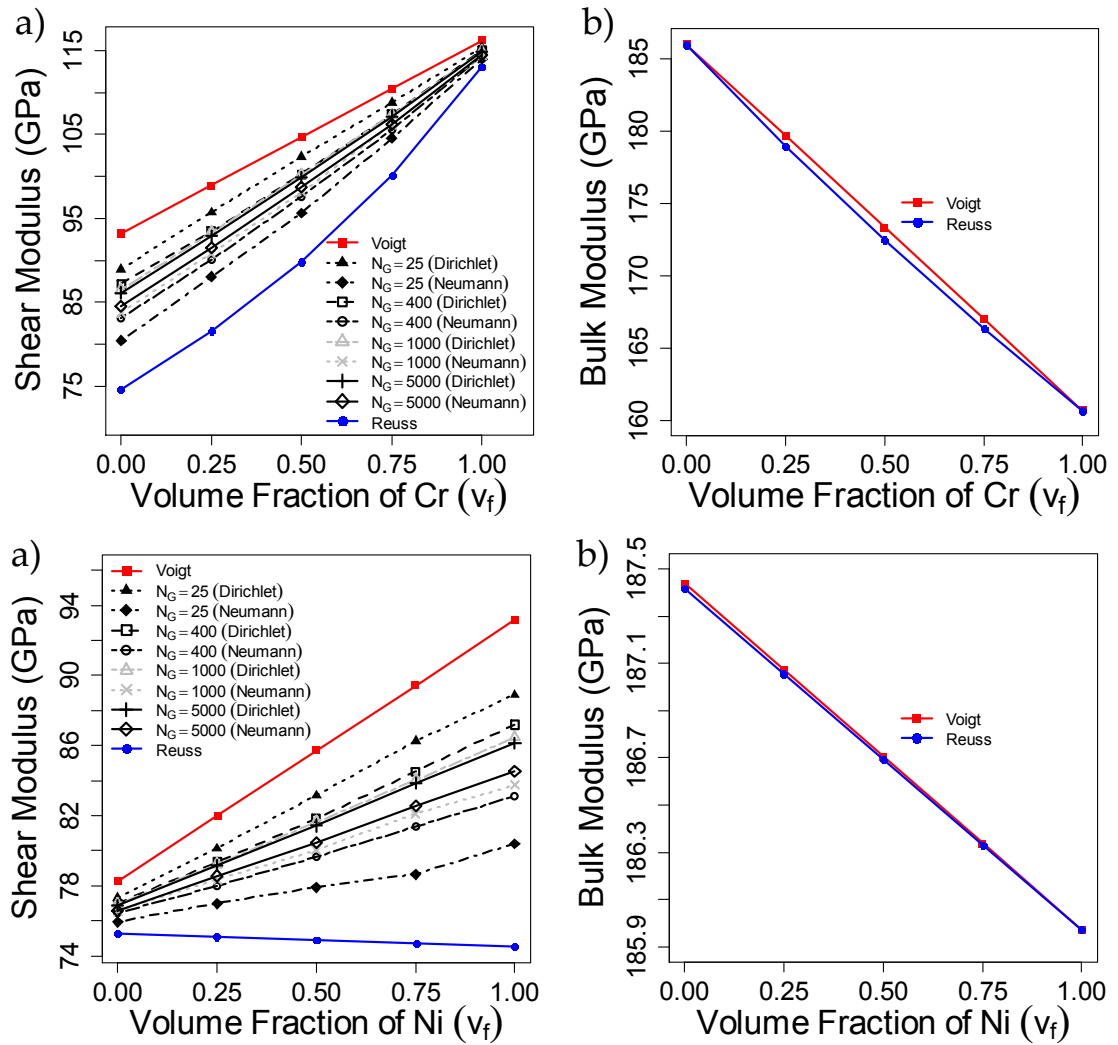


Figure 18. Bounds on elastic moduli of Ni-Cr (top) and Ni-Co (bottom) at various volume fractions: a) shear modulus (GPa) b) bulk modulus (GPa)

Let us discuss scaling behavior of all two-phase materials (Ni-Cd, Sn-Ag, Ni-Cr, Ni-Co). Fig. (19) illustrates scaling functions at various volume fractions ($v_f = 0, 0.25, 0.5, 0.75$ and 1) for these microstructures. For Ni-Cd, A_H^U is almost identical at $v_f = 0$ ($A_H^U = 1.22$) as well as $v_f = 1$ ($A_H^U = 1.25$) and therefore scaling functions are very close to each other (see Figs. 19a & e). Also, at $v_f = 0.25$ ($A_H^U = 3.77$) and $v_f = 0.75$ ($A_H^U = 3.78$), scaling functions remain the same for Ni-Cd as A_H^U is identical (see Figs. 19b & d). In addition, scaling function for Ni-Cd at $v_f = 0.5$ can be seen in Fig. (19c). Let us now consider the scaling functions for Sn-Ag. At $v_f = 0$ ($A_H^U = 1.44$) and $v_f = 1$ ($A_H^U = 1.48$), scaling functions are close to each other as A_H^U is similar (see Figs. 19a & e). Also, at $v_f = 0.25$ ($A_H^U = 1.84$) and $v_f = 0.75$ ($A_H^U = 1.85$), scaling functions are same for Sn-Ag as A_H^U is identical (see Figs. 19b & d). In addition, scaling function for Sn-Ag at $v_f = 0.5$ can be seen in Fig. (19c). It is therefore reasonable to state that scaling function depends only on ‘Heterogeneous Anisotropy Index’, A_H^U , and mesoscale, δ . By rewriting Eq. (5.2), we obtain the following

$$f(C_{(1)}^{ij}, C_{(2)}^{ij}, v_f, \delta) \equiv f(A_H^U, \delta). \quad (5.9)$$

Along similar lines, scaling trends for Ni-Cr and Ni-Co are also identical at specific volume fractions. Figs. (19b & d) show that scaling functions are close to each other for Ni-Cr at $v_f = 0.25$ and Ni-Co at $v_f = 0.75$ as A_H^U values are 1.07 and 0.98, respectively. A similar phenomenon can be observed for Ni-Cr at $v_f = 0.5$ ($A_H^U = 0.83$) and Ni-Co at $v_f = 0.5$ ($A_H^U = 0.72$) as A_H^U values are comparable (see Fig. 19c). Likewise, scaling functions are similar for Ni-Cr at $v_f = 0.75$ and Ni-Co at $v_f = 0.25$ as A_H^U values are 0.52 and 0.46, respectively (see Figs. 19d & b). In addition, scaling functions for Ni-Cr and Ni-Co at $v_f = 0$ and $v_f = 1$ can be seen in Fig. (19a) and Fig. (19e), respectively. Finally, we can also see that scaling functions are exactly the same for Ni-Cr at $v_f = 0$ (see Fig. 19a) as well as Ni-Cd and Ni-Co at $v_f = 1$ (see Fig. 19e) as $A_H^U = 1.25$ (anisotropy of single phase Ni).

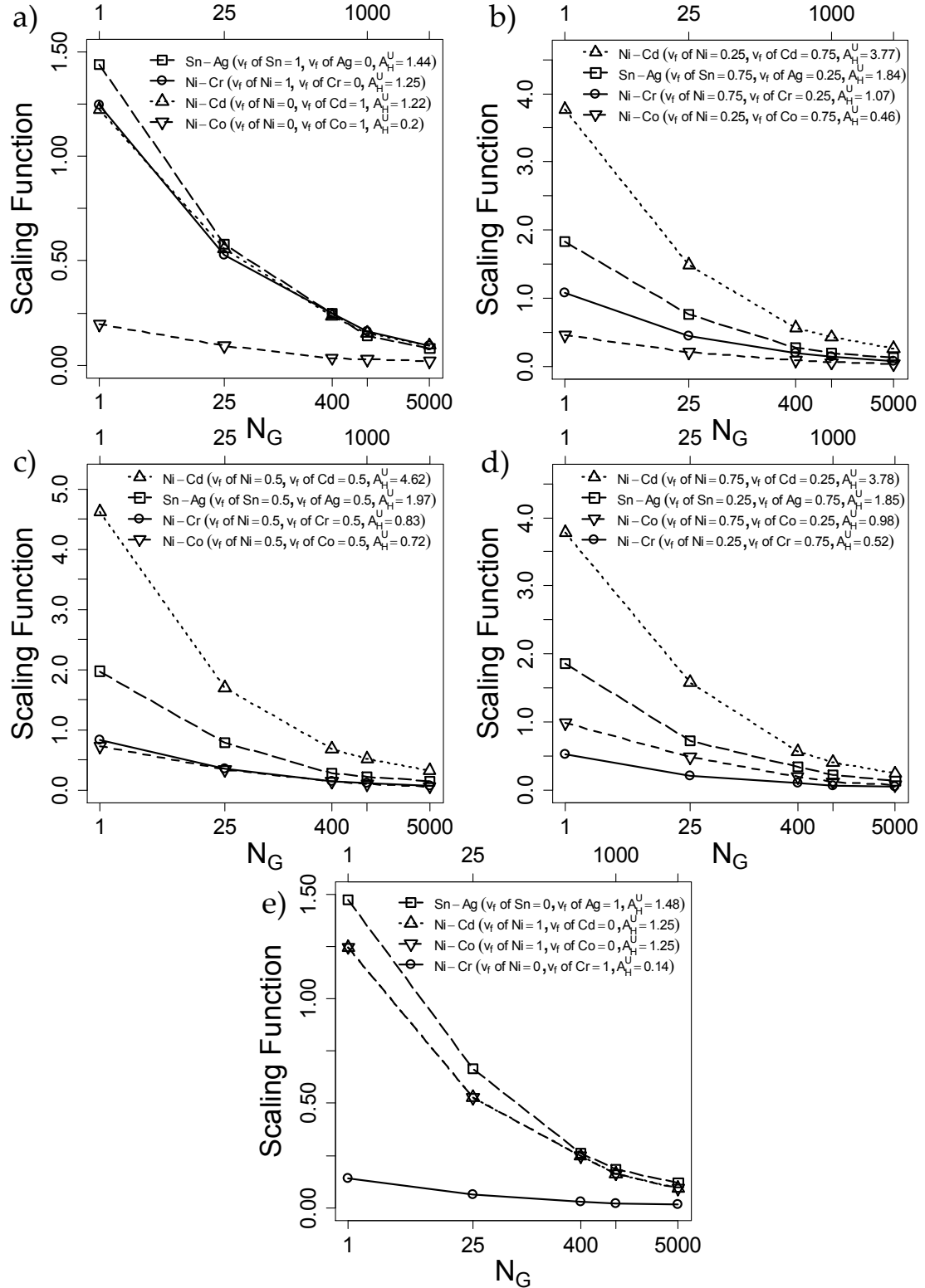


Figure 19. Scaling Function for two-phase materials: a) $v_f = 0$ b) $v_f = 0.25$ c) $v_f = 0.5$ d) $v_f = 0.75$ e) $v_f = 1$

In the next section, we demonstrate a specific form of the scaling function for any two-phase microstructure.

5.4 Constructing the Scaling Function

The functional form of the scaling function is now obtained by rewriting Eq. (5.5) as follows

$$0 \leq \frac{1}{A_H^U} f(A_H^U, \delta) \leq 1. \quad (5.10)$$

Next, we discuss the rescaled scaling function defined in Eq. (5.10). It is important to highlight that the rescaled function is similar for all two-phase materials at various volume fractions as seen in Fig. (20). Due to the finite number of realizations used to obtain ensemble averages in this study, we observe that the curves plotted in Fig. (20) are arranged in a fusiform structure, but should converge to a single curve in the limit of an infinite set of realizations.

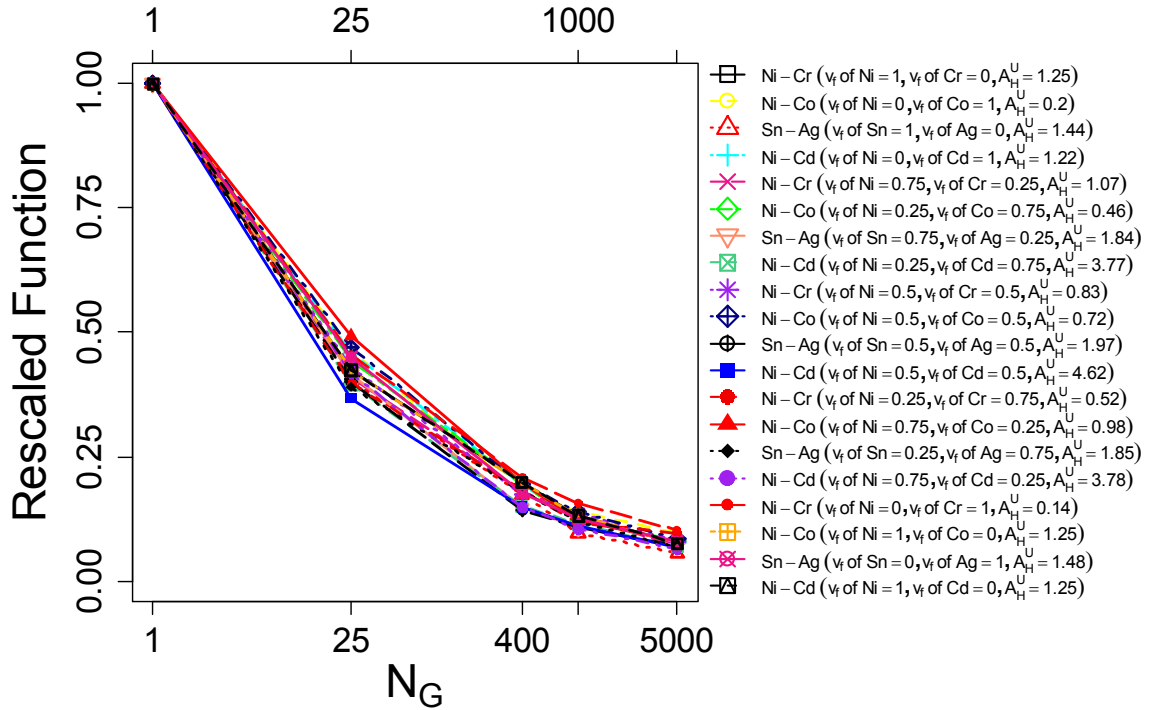


Figure 20. Rescaled Scaling Function for two-phase materials: $v_f = 0, 0.25, 0.5, 0.75, 1$

1

The rescaled function, f^* , is independent of the ‘Heterogeneous Anisotropy Index’, A_H^U , and is only a function of the mesoscale, δ . It is also worthwhile to mention that the existence of such a f^* is equivalent to stating that f is proportional to A_H^U . By redefining the scaling function, the following is obtained

$$f(A_H^U, \delta) = A_H^U f^*(\delta). \quad (5.11)$$

Let us now take the average values of $f^*(\delta)$ from Fig. (20) in order to develop the effective mean rescaled function (obtained through numerical simulations) and curve fit it (see Fig. 21).

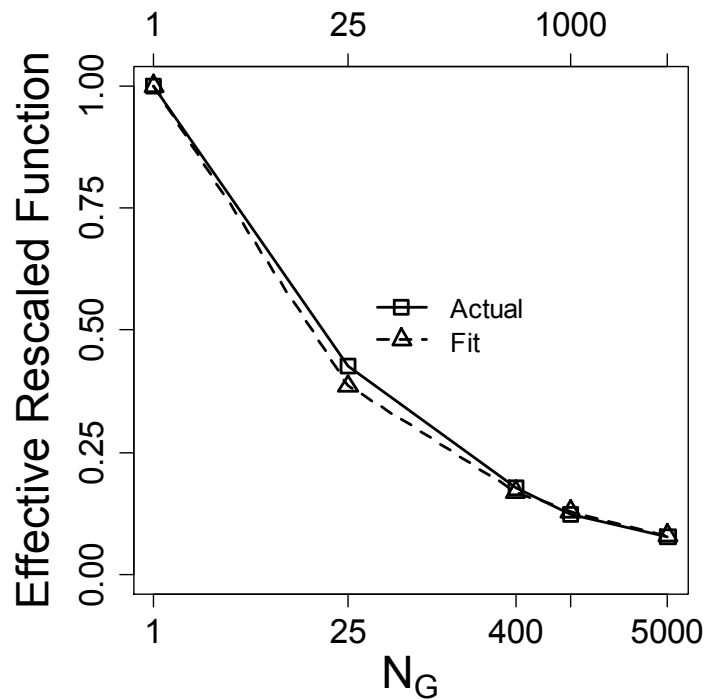


Figure 21. Effective Rescaled Scaling Function & Fit for two-phase materials

It is now possible to show the following form of $f^*(\delta)$ which is based on the effective function and its fit

$$f^*(\delta) = (\delta)^{-0.89}. \quad (5.12)$$

By using Eqs. (5.11) and (5.12), we obtain the scaling function

$$f(A_H^U, \delta) = A_H^U(\delta)^{-0.89}, \quad \delta = (N_G)^{\frac{1}{3}}. \quad (5.13)$$

At this stage, we reconstruct the scaling function using Eq. (5.13) for all two-phase polycrystals (Ni-Cd, Sn-Ag, Ni-Cr, Ni-Co) at different volume fractions ($v_f = 0, 0.25, 0.5, 0.75, 1$) as shown in Fig. (22). It is evident from this plot that this formulation captures the scaling function accurately for all two-phase materials at several volume fractions.

5.5 Material Scaling Diagram

The power-law form of scaling function given in Eq. (5.13) is employed in order to construct contours in (A_H^U, N_G) space as shown in Fig. (23). For any two-phase material, the number of grains (N_G) required for homogenization can be obtained by choosing a value of scaling function within the interval ($0.01 \leq f \leq 0.23$). It is also clear that the curves shift towards higher grain sizes as scaling function decreases (from $f = 0.23$ to $f = 0.01$) and vice-versa. We have also seen that scaling function is zero at infinite grain sizes. It is now possible to select a specific value of scaling function in order to determine the grain sizes required for homogenization. We illustrate this concept by choosing a finite value of scaling function ($f = 0.2$) and develop Fig. (24) for several two-phase materials (Ni-Cd, Sn-Ag, Ni-Cr, Ni-Co) at various volume fractions ($v_f = 0, 0.25, 0.5, 0.75, 1$). It is observed that, for a highly anisotropic two-phase material (Ni-Cd with $A_H^U = 4.62$), homogeneity can be achieved at $N_G = 39835$ ($\delta \cong 35$). Similarly, for Sn-Ag at $v_f = 0.5$ and $A_H^U = 1.97$, aggregate response can be determined at $N_G = 2255$ ($\delta \cong 14$). Finally, for a two-phase polycrystal with low anisotropy (Ni-Cr with $A_H^U = 0.14$), the number of grains required for homogenization is $N_G = 1$ ($\delta = 1$).

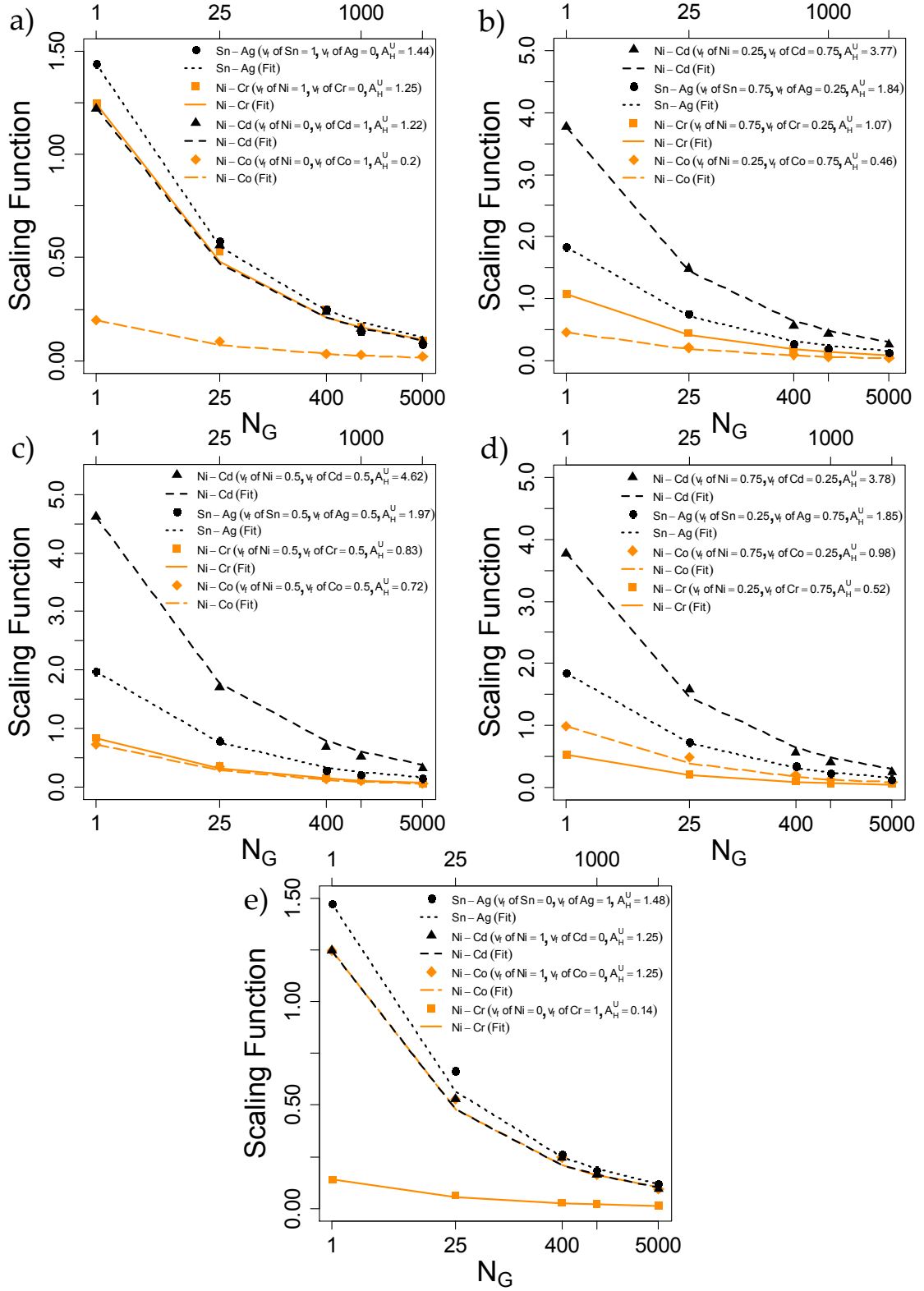


Figure 22. Scaling Function & Fit for two-phase materials: a) $v_f = 0$ b) $v_f = 0.25$ c) $v_f = 0.5$ d) $v_f = 0.75$ e) $v_f = 1$

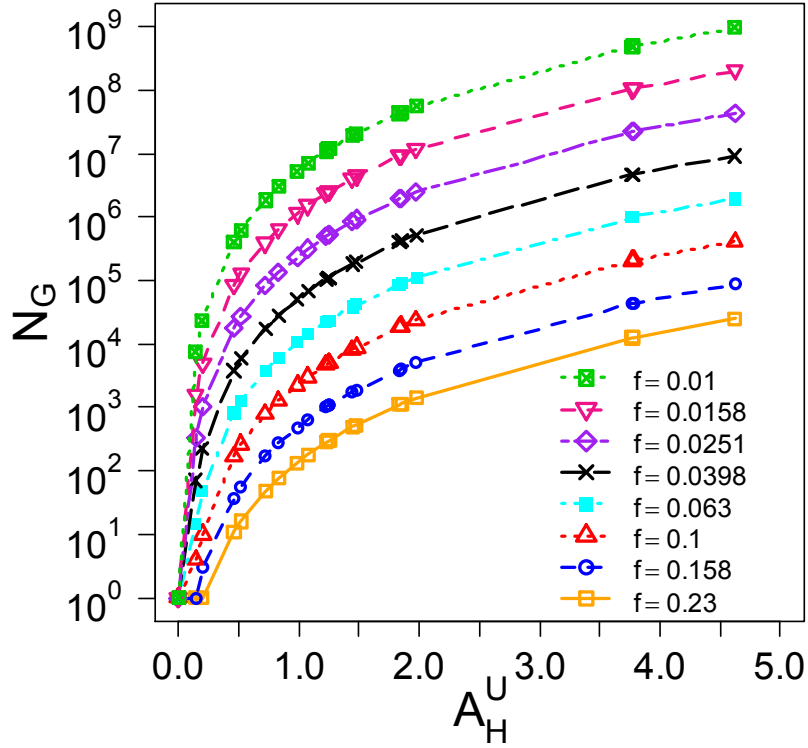


Figure 23. Contours of Scaling Function for $0.01 \leq f \leq 0.23$

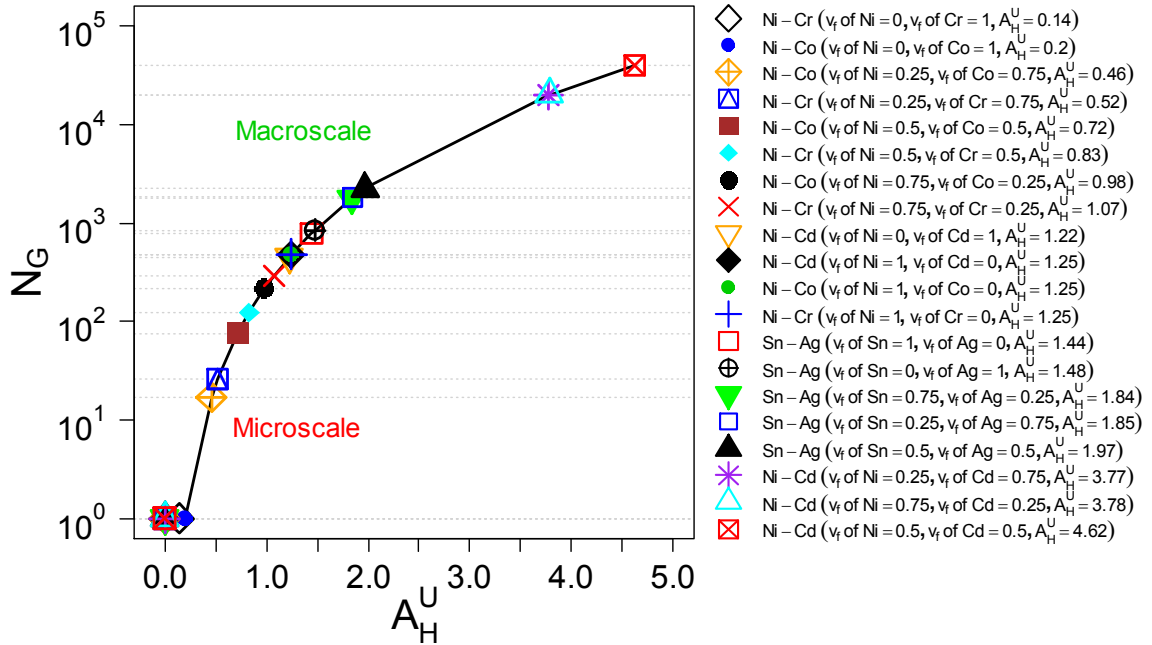


Figure 24. Material Scaling Diagram at $f = 0.2$ (two-phase materials)

5.6 Summary

In chapter 5, we have illustrated the procedure to obtain scale-dependent bounds on the elastic response of two-phase random polycrystals by solving Dirichlet and Neumann type boundary value problems (9250) which are consistent with the Hill-Mandel homogenization condition. It was also shown that a variety of two-phase materials at different volume fractions can be studied together in terms of the elastic scaling function. This form of the scaling function consists of the 'Heterogeneous Anisotropy Index, A_H^U ' and the number of grains in the microstructure. It was also shown that A_H^U behaves as the Universal Anisotropy Index when the volume fractions are 0 and 1. Finally, we developed a material scaling diagram for any two-phase material which can be used for estimating the grain size required for homogenization. For single and two-phase polycrystals, the functional form of the scaling function has been established so far in terms of the single crystal properties and the mesoscale. In the next chapter, we attempt to develop a deeper understanding of the scaling function by examining analogies with dimensionless numbers.

Chapter 6

Scaling Function in Mechanics of Random Materials

Dimensionless numbers play a vital role in the mechanics of continuous media. Traditionally, dimensionless numbers have been more widely used in fluid mechanics and heat transfer (e.g. Reynolds Number, Knudsen Number, Peclet Number, Fourier Number, etc.) when compared to the mechanics of solids. The objective of this research is to introduce the notion of a dimensionless scaling function and highlight its importance in the multi-scale scaling behavior of a variety of composite materials from 2D checkerboard microstructures to 3D polycrystals. It is demonstrated that the scaling function quantifies the departure of a random heterogeneous medium from a homogeneous continuum. Furthermore, a generic form of the scaling function is presented as a function of the phase contrast (k), volume fraction (v_f), Universal Anisotropy Index (A^U) and mesoscale (δ). Application problems include elasticity, thermal conductivity, electrical conductivity and viscoelasticity⁴.

6.1 Introduction

In this study, the notion of a scaling function is introduced that is analogous to the definition of dimensionless numbers that are widely used in several fields including fluid mechanics [89], electromagnetism [90], astrophysics [91], medicine [92, 93, 94] and pharmacy [95]. Recently, a combination of dimensionless numbers such as non-dimensional heat input, Peclet number (ratio of convective to diffusive transport [96]), Marangoni number (ratio of surface tension force to viscous force [97]) and Fourier number (ratio of heat transfer by conduction to rate of energy stored [98]) was used to analyze the structure-property relationship of 3D printed materials (see Mukherjee et al. [99]). The proposed scaling function stems from the scalar

⁴See also [88] S. I. Ranganathan and M. R. Murshed, "Scaling function in mechanics of random materials," *Encyclopedia of Continuum Mechanics*, accepted, 2017

contraction of the ensemble averaged tensors obtained using Dirichlet and Neumann type boundary conditions. In its most generic form, the scaling function depends upon the phase contrast, volume fraction, material anisotropy and mesoscale. The scaling function by definition quantifies the departure of a random medium from a homogeneous continuum. In the subsequent sections, a functional form for the scaling function will be introduced that is applicable to a wide range of composite materials (two-phase checkerboards, two-phase correlated microstructures and 3D polycrystals).

6.2 Notion of a Scaling Function

The functional form of the scaling function depends upon the specific microstructure under investigation. Within the scope of this research, four microstructures are considered—i) Uncorrelated random checkerboard (see Fig. 25a); ii) Correlated two-phase microstructure (see Fig. 25b); iii) two-phase viscoelastic composite (see Fig. 25c) and iv) random polycrystal (see Fig. 25d).

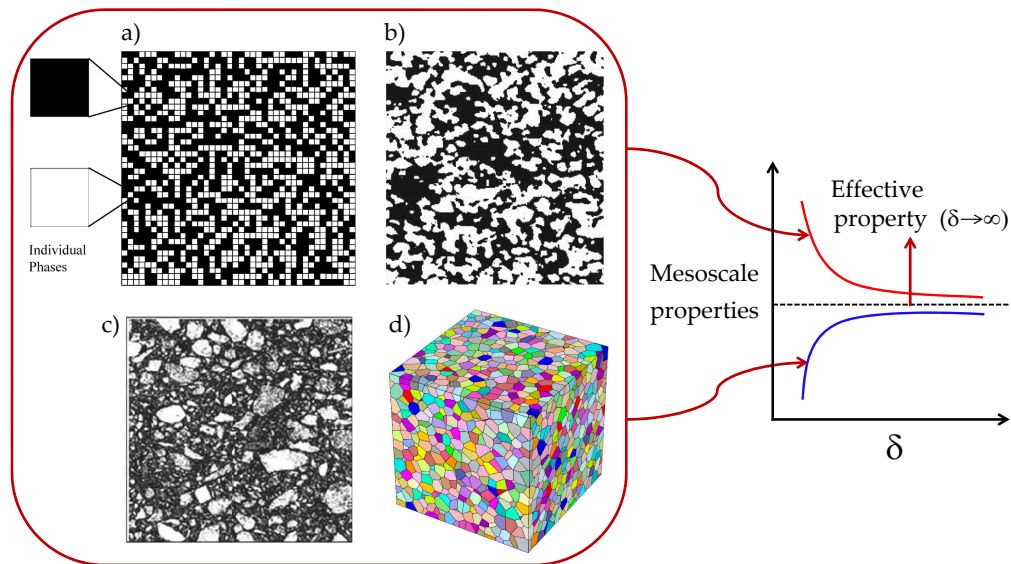


Figure 25. Homogenization Methodology: a) Checkerboard microstructure in thermal conductivity [11, 55], elasticity [9] and electrical conductivity [13]; b) two-phase ($\text{Al}_2\text{O}_3\text{-Ni}$) microstructure in thermal conductivity [46]; c) microstructure of a viscoelastic material (mixture of asphalt and concrete) [56]; d) polycrystal in 3D elasticity (color represents random orientation of each grain) [40]

In order to identify the specific forms of the scaling function, a methodology based on the Hill-Mandel homogenization condition is employed (see Fig. 25). These forms include the dependence of scaling function on phase contrast (f_1), volume fraction (f_2), anisotropy measure (f_3) and mesoscale (f_4). Next, the microstructures are subjected to Dirichlet and Neumann type boundary conditions that result in rigorous scale-dependent bounds with increasing mesoscales (δ). For a given realization, $\omega(\in \Omega)$, the Dirichlet boundary condition results in a mesoscale random stiffness tensor, $C_\delta^d(\omega)$, and the Neumann boundary condition results in a mesoscale random compliance tensor, $S_\delta^n(\omega)$, for linear elastic materials. In the context of heat or electrical conductivity, $C_\delta^d(\omega)$ [$S_\delta^n(\omega)$] represents the second-rank conductivity [resistivity] tensors and for viscoelastic materials, they represent the complex modulus [compliance] tensors, respectively. These tensors are inverse of each other in the limit $\delta \rightarrow \infty$. The scaling function in its most generic form is defined as follows

$$f = \langle \mathbf{C}_\delta^d \rangle : \langle \mathbf{S}_\delta^n \rangle - \langle \mathbf{C}_\infty^d \rangle : \langle \mathbf{S}_\infty^n \rangle, \quad (6.1)$$

where the operators $:$ and $\langle \bullet \rangle$, indicate tensor contraction and ensemble averaging over the realization space, respectively. It turns out that Eq. (6.1) takes the following generic form for all microstructures investigated

$$f = cf_1(k)f_2(v_f)f_3(A)f_4(\delta), \quad (6.2)$$

where c is a constant, k is phase contrast, v_f is volume fraction, A is an anisotropy measure and δ is mesoscale. In the subsequent sections, the functional form of each of the terms appearing in Eq. (6.2) will be discussed.

6.2.1. Effect of phase contrast, k , on scaling function. The phase contrast, k , quantifies the mismatch in the material properties of a composite material.

For a 2D microstructure, $k = \frac{c_1}{c_2}$, where c_1 and c_2 correspond to the conductivities (thermal or electrical conductivity) for phase 1 and phase 2, respectively. For 3D polycrystals with uniaxial thermal character, $k = \frac{c_1}{c_3}$, where c_1 and c_3 correspond to ratio of the two independent principal conductivities of the single crystal. The dependence of scaling function on the contrast can now be expressed as follows

$$f_1(k) = \left(\sqrt{k} - \frac{1}{\sqrt{k}} \right)^2. \quad (6.3)$$

Fig. (26) illustrates the phase contrasts ($k = 0.01, 0.1, 1, 10, 100$) for two-phase checkerboards, two-phase correlated microstructures and 3D polycrystals. It is evident that the phase contrast has the same effect on scaling function for all applications. Also, scaling function does not distinguish between k and k^{-1} and, therefore, microstructures with phase contrasts k or k^{-1} scale identically.

6.2.2. Effect of volume fraction, v_f , on scaling function. In this section, the effect of volume fraction, v_f (amount of phase 1 in the entire volume) on the scaling function is examined. Clearly, the volume fraction always ranges between zero and one ($0 \leq v_f \leq 1$), with the limiting values representing a homogeneous material. The following is the dependence of scaling function on the volume fraction

$$f_2(v_f) = v_f(1 - v_f). \quad (6.4)$$

Fig. (27) illustrates the effect of volume fraction on $f_2(v_f)$ for a two-phase checkerboard in electrical conductivity. It is clear that the scaling function value is largest [$f_2(v_f) = 0.25$] at $v_f = 0.5$. This is due to the fact that at 50% volume fraction, level of heterogeneity is largest in a given microstructure (see Raghavan et al. [13]).

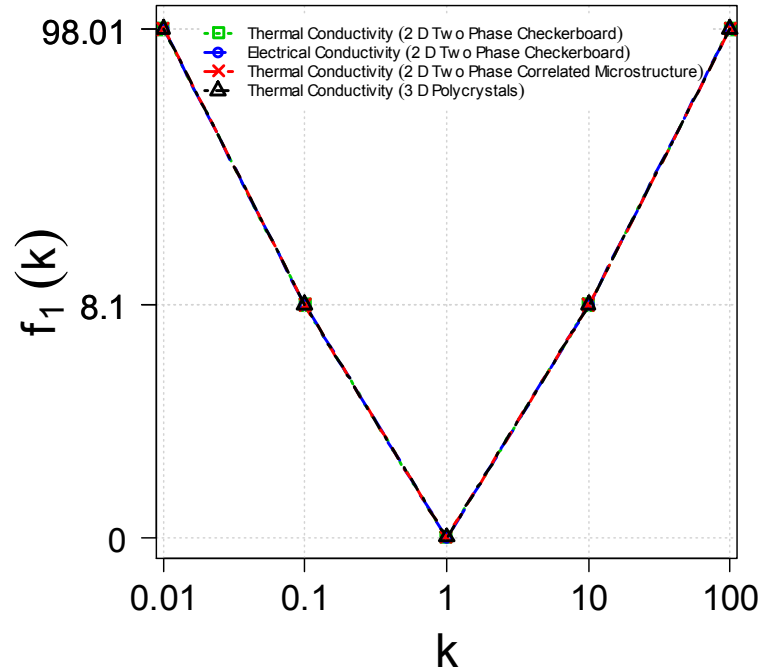


Figure 26. $f_1(k)$ vs. Phase Contrast, k : i) 2D Two Phase Checkerboard (Thermal Conductivity [55] and Electrical Conductivity [13]); ii) 2D Two Phase Correlated Microstructure (Thermal Conductivity [46]); iii) 3D Polycrystals (Thermal Conductivity [12])

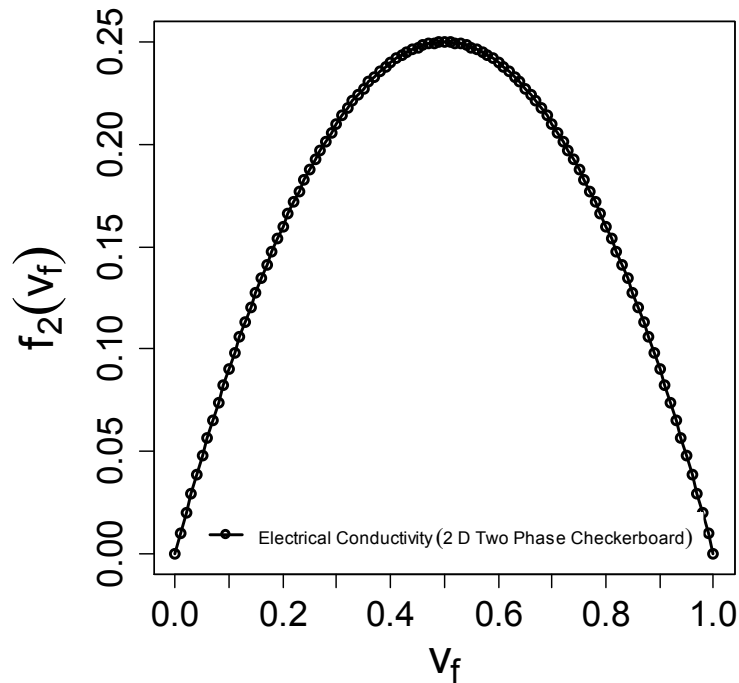


Figure 27. $f_2(v_f)$ vs. Volume Fraction, v_f , in Electrical Conductivity

6.2.3. Effect of an anisotropy measure, A , on scaling function.

Material anisotropy of the microstructure plays an important role in the definition of the scaling function. The effect of anisotropy, A , on the scaling function depends upon the specific microstructure under investigation. For single phase 3D polycrystals, this dependence is as follows

$$f_3(A) = A^U = 5 \frac{G^V}{G^R} + \frac{K^V}{K^R} - 6, \quad (6.5)$$

where A^U is the Universal Anisotropy Index [22], G is shear modulus, K is bulk modulus, V is Voigt estimate [66], R is Reuss estimate [67]. Along similar lines, for 2D two-phase elastic microstructures, $f_3(A)$ takes the following form (see Raghavan and Ranganathan [9])

$$f_3(A) = 2 \frac{G^V}{G^R} + \frac{K^V}{K^R} - 3. \quad (6.6)$$

More recently, Zhang and Ostoja-Starzewski [56] examined the scaling of 2D viscoelastic composites and proposed the following form for $f_3(A)$

$$f_3(A) = 2\mu_{2D}^{*V}(\gamma)J_{2D}^{*R}(\gamma) + k_{2D}^{*V}(\gamma)L_{2D}^{*R}(\gamma) - 3, \quad (6.7)$$

where γ is the frequency, μ_{2D}^* is the relaxation shear modulus, J_{2D}^* is the complex shear compliance, k_{2D}^* is the relaxation bulk modulus and L_{2D}^* is the complex bulk compliance.

6.2.4. Effect of mesoscale, δ , on scaling function. The mesoscale (δ) can be defined as (see Ranganathan and Ostoja-Starzewski [19])

$$\delta = \frac{l}{d}, \quad (6.8)$$

where l is the length scale of observation (domain size) and d is the characteristic

length scale (for example the grain size). For 3D polycrystals, $\delta = (N_G)^{\frac{1}{3}}$. Under limiting values of the mesoscale, δ , the scaling function takes an exact form

$$f_4(\delta \approx \infty) = 0. \quad (6.9)$$

In addition, the following rigorous bounds on scaling function can be established at finite mesoscales

$$f_4(\delta \approx \infty) \leq f_4(\delta') \leq f_4(\delta) \leq f_4(\delta = 1) \quad \forall 1 \leq \delta \leq \delta' \leq \infty. \quad (6.10)$$

Extensive numerical simulations on a variety of composite materials by several authors (see Raghavan et al. [13], Dalaq et al. [55], Kale et al. [46], Ranganathan and Ostoja-Starzewski [12], Raghavan and Ranganathan [9], Ranganathan and Ostoja-Starzewski [19], Murshed and Ranganathan [40], Zhang and Ostoja-Starzewski [56]) resulted in the following empirical forms for the function $f_4(\delta)$

$$f_4(\delta) = \exp[B(\delta - 1)^C], \quad (6.11a)$$

$$f_4(\delta) = \delta^D, \quad (6.11b)$$

$$f_4(\delta) = \frac{e}{(f + \frac{\delta}{\lambda})^n}, \quad (6.11c)$$

where B , C , D , e , f , λ and n are arbitrary constants relevant to the specific microstructure being investigated and is discussed in the following section.

6.3 Application Problems

In this section, the functional form of the scaling function is summarized for a variety of applications. These include Conductivity in 2D two-phase random and correlated microstructures, Conductivity in 3D polycrystals, Elasticity in 2D two-phase checkerboards, Elasticity in 3D polycrystals and Viscoelasticity in 2D

two-phase checkerboards.

6.3.1. Conductivity in 2D two-phase microstructures. Consider 2D two-phase microstructures either conducting heat (or electricity) as illustrated in Fig. (25a & b). One of the microstructure is a random checkerboard and the other is a gaussian correlated microstructure. In order to establish the functional form of the scaling function, they were subjected to temperature (electric field) and heat flux (current density) boundary conditions. The boundary value problems were then set up and solved over several realizations to extract the mesoscale random conductivity and resistivity tensors. The procedure was repeated for a variety of material combinations and subsequently, Eq. (6.1) was used to establish the following form of the scaling function (see Dalaq et al. [55], Raghavan et al. [13] and Kale et al. [46])

$$f = cf_1(k)f_2(v_f)f_3(A)f_4(\delta), \quad (6.12a)$$

and

$$\begin{aligned} c &= 2, \\ f_1(k) &= \left(\sqrt{k} - \frac{1}{\sqrt{k}} \right)^2, \\ f_2(v_f) &= v_f(1 - v_f), \\ f_3(A) &= 1, \\ f_4(\delta) &= \exp[B(\delta - 1)^C] \quad (\text{random microstructure}), \\ f_4(\delta) &= \frac{e}{(f + \frac{\delta}{\lambda})^n} \quad (\text{correlated microstructure}). \end{aligned} \quad (6.12b)$$

Dalaq et al. [55] studied random checkerboards at 50% volume fractions and empirically determined the constants B , C to be -0.53 and 0.69, respectively. In a subsequent study, Raghavan et al. [13] accounted for all volume fractions and proposed $B = -0.73$ and $C = 0.50$. In a more recent study, Kale et al. [46] analyzed a two-phase Gaussian correlated microstructure ($\text{Al}_2\text{O}_3\text{-Ni}$) which was generated by

using an appropriate threshold for the desired volume fraction on a continuous Gaussian correlated random field. The authors obtained the following constants: $e = 3.70$, $f = 1.90$, $\lambda = 1$ and $n = 1.23$.

6.3.2. Conductivity in 3D polycrystals. The microstructure used for determining thermal conductivity in 3D polycrystals is similar to Fig. (25d), albeit with cubic shaped grains. By applying temperature and heat flux boundary conditions on the polycrystal, and by employing a similar procedure as described in section 6.3.1., results in the functional form for the scaling function (see Ranganathan and Ostoja-Starzewski [12])

$$f = cf_1(k)f_2(v_f)f_3(A)f_4(\delta), \quad (6.13a)$$

and

$$\begin{aligned} c &= \frac{2}{3}, \\ f_1(k) &= \left(\sqrt{k} - \frac{1}{\sqrt{k}} \right)^2, \\ f_2(v_f) &= 1, \\ f_3(A) &= 1, \\ f_4(\delta) &= \exp[-0.91(\delta - 1)^{0.50}]. \end{aligned} \quad (6.13b)$$

6.3.3. Elasticity in 2D two-phase checkerboards. A two-phase random checkerboard is illustrated in Fig. (25a). Much of the numerical procedure remains the same as described in section 6.3.1. The main difference is that the temperature and heat flux boundary conditions are replaced with the displacement and traction boundary conditions, respectively. The resulting mesoscale random stiffness and compliance tensors turn out to be tensors of rank four unlike the second rank conductivity (or resistivity) tensor. Based on extensive numerical simulations, the scaling function takes the following form (see Raghavan and Ranganathan [9])

$$f = cf_1(k)f_2(v_f)f_3(A)f_4(\delta), \quad (6.14a)$$

and

$$\begin{aligned} c &= 1, \\ f_1(k) &= 1, \\ f_2(v_f) &= 1, \\ f_3(A) &= 2\frac{G^V}{G^R} + \frac{K^V}{K^R} - 3, \\ f_4(\delta) &= \exp[-0.58(\delta - 1)^{0.44}]. \end{aligned} \quad (6.14b)$$

6.3.4. Elasticity in 3D polycrystals. Consider 3D random polycrystals as shown in Fig. (25d). Microstructures using Voronoi tessellations were generated in the software Neper [33] by Murshed and Ranganathan [40], whereas Ranganathan and Ostoja-Starzewski [19] considered cubic shaped grains. Employing a similar procedure as described in section 6.3.3., results in the following form for the scaling function

$$f = cf_1(k)f_2(v_f)f_3(A)f_4(\delta), \quad (6.15a)$$

and

$$\begin{aligned} c &= 1, \\ f_1(k) &= 1, \\ f_2(v_f) &= 1, \\ f_3(A) &= A^U = 5\frac{G^V}{G^R} + \frac{K^V}{K^R} - 6, \\ f_4(\delta) &= \exp[-0.77(\delta - 1)^{0.50}], \\ f_4(\delta) &= \delta^{-0.89}. \end{aligned} \quad (6.15b)$$

A stretched exponential form was obtained for $f_4(\delta)$ by Ranganathan and Ostoja-Starzewski [19] who considered only crystals belonging to cubic symmetry. However, Murshed and Ranganathan [40] conducted simulations on all crystal classes

(from cubic to triclinic) and proposed a power-law relation for $f_4(\delta)$.

6.3.5. Viscoelasticity in 2D two-phase checkerboards. The viscoelastic composite material considered is shown in Fig. (25c). These microstructures were subjected to displacement and traction boundary conditions. Subsequently, the boundary value problems were set up and solved over several realizations in order to extract the mesoscale random complex modulus and complex compliance tensors. The following form of the scaling function was then determined (see Zhang and Ostoja-Starzewski [56])

$$f = cf_1(k)f_2(v_f)f_3(A)f_4(\delta), \quad (6.16a)$$

and

$$\begin{aligned} c &= 1, \\ f_1(k) &= 1, \\ f_2(v_f) &= 1, \\ f_3(A) &= f_3(A) = 2\mu_{2D}^{*V}(\gamma)J_{2D}^{*R}(\gamma) + k_{2D}^{*V}(\gamma)L_{2D}^{*R}(\gamma) - 3, \\ f_4(\delta) &= \exp[-0.45(\delta - 1)^{0.66}]. \end{aligned} \quad (6.16b)$$

The scaling functions for all the materials considered are summarized in Fig. (28). Clearly, it can be seen that the scaling function approaches zero with increasing mesoscales.

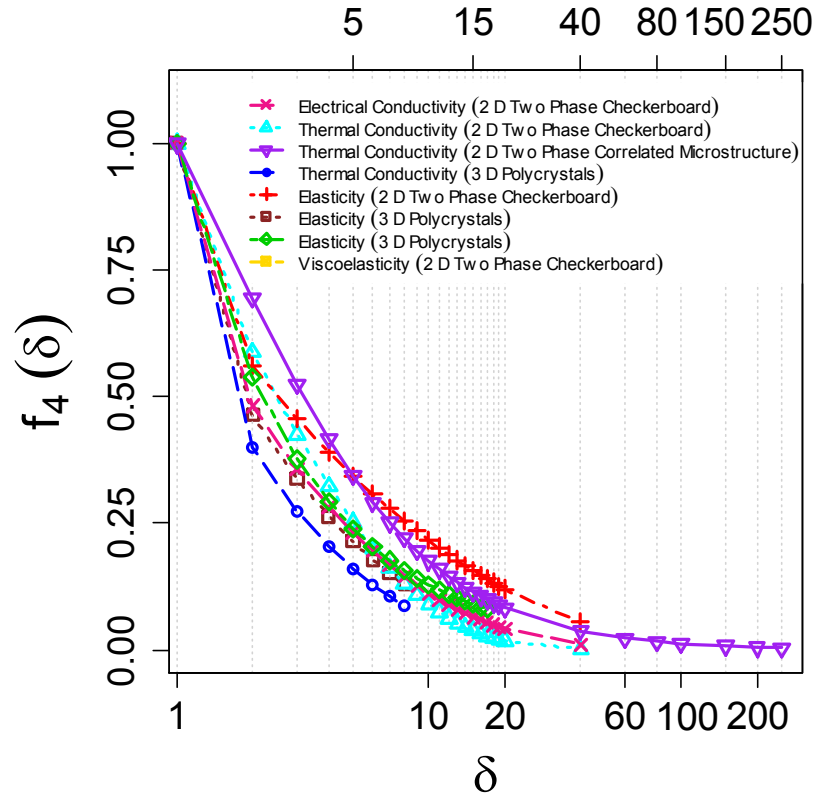


Figure 28. $f_4(\delta)$ vs. Mesoscale, δ , for several applications: a) Electrical Conductivity (2D Two Phase Checkerboard) [13]; b) Thermal Conductivity (2D Two Phase Checkerboard) [55]; c) Thermal Conductivity (2D Two Phase Correlated Microstructure) [46]; d) Thermal Conductivity (3D Polycrystals) [12]; e) Elasticity (2D Two Phase Checkerboard) [9]; f) Elasticity (3D Polycrystals) [19]; g) Elasticity (3D Polycrystals) [40]; h) Viscoelasticity (2D Two Phase Checkerboard) [56]

6.4 Summary

Dimensionless numbers play an important role in a variety of problems in physics and engineering. In this context, the concept of a scaling function is introduced and its generic form is proposed based on the studies of a variety of composites. The extent of heterogeneity (phase contrast, volume fraction) and anisotropy in the microstructure contributes significantly to the scaling function. The scaling function also strongly depends on the mesoscale, with good curve-fitting models obtained on the basis of extensive numerical simulations. The scaling function essentially quantifies the departure of a random medium from a homogeneous continuum.

Chapter 7

Conclusions and Future Research Directions

In this dissertation, we developed unifying scaling laws that describe the response of single and two-phase random polycrystals with individual grains belonging to arbitrary crystal class (from cubic to triclinic).

In chapter 2, a mathematical formulation was developed for the elastic scaling function and the theory for obtaining rigorous scale-dependent bounds was discussed. We also illustrated the methodology for solving Dirichlet and Neumann type boundary value problems.

Subsequently, scale-dependent bounds on the elastic response of single phase polycrystals were obtained in chapter 3. Some important properties of the elastic scaling function was then discussed and we derived its power-law form by numerical simulations. This specific form of the scaling function was determined in terms of the Universal Anisotropy Index, A^U , and the mesoscale, δ . By selecting a finite value of the scaling function, a material scaling diagram was constructed using which the grain size required for homogenization can be estimated.

Next, we considered polycrystalline materials with highly anisotropic single crystals belonging to lower symmetry class. A versatile methodology based on the Hill-Mandel homogenization condition and variational principles in elasticity was highlighted in chapter 4. This framework was employed to obtain tighter bounds on monoclinic and triclinic materials as compared to all other methods proposed in the literature.

In Chapter 5, we extended the concept of an elastic scaling function to study the mesoscale constitutive response of two-phase polycrystals. In doing so, we introduced the notion of a ‘Heterogeneous Anisotropy Index, A_H^U ’ and examined its role on the finite-size scaling of material properties. It turns out that A_H^U is

a function of 43 variables and it behaves as A^U under certain limiting conditions (volume fractions 0 and 1). Subsequently, the power-law form of the scaling function was obtained in terms of A_H^U and δ . Based on the scaling function, a material scaling diagram was developed which captures the convergence to the effective properties for any two-phase material.

After developing the functional form of the scaling function for single and two-phase polycrystals, the analogy of scaling function to dimensionless numbers was established in chapter 6. A generic form of the scaling function was proposed based on the studies of a variety of composite materials. It was demonstrated that the scaling function depends upon heterogeneity (phase contrast, volume fraction) and material anisotropy in the microstructure. Also, the mesoscale plays a fundamental role in the definition of the scaling function. In essence, the scaling function quantifies the departure of a random medium from a homogeneous continuum.

On a final note, the concepts demonstrated in this dissertation can be extended to other applications including electrical conduction, electrostatics, elastic wave propagation, piezoelectricity, magnetostatics and diffusion. Also, we have analyzed only two of the three boundary conditions that stem from the Hill-Mandel condition. One can also analyze the elastic response of materials subjected to the mixed-orthogonal boundary condition. In this study, we have only considered single and two-phase materials which can be extended to include microstructures with multiple (more than two) phases. Further, an alternate approach to the current work is to perform multiscale analysis using machine learning (see Koutsourelakis [100]). This approach has been investigated in applications including quantum physics [101] and quantum chemistry [102]. In fact, such topics are of great importance for analyzing the scaling behavior of composite materials. However, they are beyond the scope of this dissertation.

References

- [1] T. Belytschko, T. Hughes, N. Patankar, C. Herakovich, and C. Bakis, “Research directions in computational and composite mechanics,” *A report of the United States National Committee on Theoretical and Applied Mechanics*, 2007.
- [2] J. T. Oden, T. Belytschko, I. Babuska, and T. Hughes, “Research directions in computational mechanics,” *Computer Methods in Applied Mechanics and Engineering*, vol. 192, no. 7, pp. 913–922, 2003.
- [3] M. R. Murshed, S. I. Ranganathan, and F. H. Abed, “Design maps for fracture resistant functionally graded materials,” *European Journal of Mechanics - A/Solids*, vol. 58, pp. 31–41, 2016. [Online]. Available: <https://doi.org/10.1016/j.euromechsol.2016.01.002>
- [4] M. Mehrali, S. T. Latibari, M. Mehrali, H. S. C. Metselaar, and M. Silakhori, “Shape-stabilized phase change materials with high thermal conductivity based on paraffin/graphene oxide composite,” *Energy Conversion and Management*, vol. 67, pp. 275–282, 2013.
- [5] R. Z. Valiev, M. Y. Murashkin, and I. Sabirov, “A nanostructural design to produce high-strength Al alloys with enhanced electrical conductivity,” *Scripta Materialia*, vol. 76, pp. 13–16, 2014.
- [6] C. C. Mei and B. Vernescu, *Homogenization methods for multiscale mechanics*. World Scientific, 2010.
- [7] R. Hill, “Elastic properties of reinforced solids: some theoretical principles,” *Journal of the Mechanics and Physics of Solids*, vol. 11, no. 5, pp. 357–372, 1963.
- [8] J. Mandel, “Contribution théorique à l’étude de l’érouissage et des lois de l’écoulement plastique,” in *Applied Mechanics*. Springer, 1966, pp. 502–509.
- [9] B. V. Raghavan and S. I. Ranganathan, “Bounds and scaling laws at finite scales in planar elasticity,” *Acta Mechanica*, vol. 225, no. 11, pp. 3007–3022, 2014.
- [10] S. I. Ranganathan and M. Ostojca-Starzewski, “Towards scaling laws in random polycrystals,” *International Journal of Engineering Science*, vol. 47, no. 11, pp. 1322–1330, 2009.
- [11] A. S. Dalaq and S. I. Ranganathan, “Invariants of mesoscale thermal conductivity and resistivity tensors in random checkerboards,” *Engineering Computations*, vol. 32, no. 6, pp. 1601–1618, 2015.
- [12] S. I. Ranganathan and M. Ostojca-Starzewski, “Mesoscale conductivity and scaling function in aggregates of cubic, trigonal, hexagonal, and tetragonal crystals,” *Physical Review B*, vol. 77, no. 21, p. 214308, 2008.

- [13] B. V. Raghavan, S. I. Ranganathan, and M. Ostoja-Starzewski, “Electrical properties of random checkerboards at finite scales,” *AIP Advances*, vol. 5, no. 1, p. 017131, 2015.
- [14] X. Du and M. Ostoja-Starzewski, “On the scaling from statistical to representative volume element in thermoelasticity of random materials,” *Networks and Heterogeneous Media*, vol. 1, no. 2, pp. 259–274, 2006.
- [15] M. Ostoja-Starzewski, “Material spatial randomness: From statistical to representative volume element,” *Probabilistic Engineering Mechanics*, vol. 21, no. 2, pp. 112–132, 2006.
- [16] M. Ostoja-Starzewski, X. Du, Z. Khisaeva, and W. Li, “Comparisons of the size of the representative volume element in elastic, plastic, thermoelastic, and permeable random microstructures,” *International Journal for Multiscale Computational Engineering*, vol. 5, no. 2, pp. 73–82, 2007.
- [17] X. Du and M. Ostoja-Starzewski, “On the size of representative volume element for darcy law in random media,” in *Proceedings of the Royal Society of London A: Mathematical, Physical and Engineering Sciences*, vol. 462, no. 2074, 2006, pp. 2949–2963.
- [18] M. Ostoja-Starzewski, *Microstructural Randomness and Scaling in Mechanics of Materials*. CRC Press, 2007.
- [19] S. I. Ranganathan and M. Ostoja-Starzewski, “Scaling function, anisotropy and the size of RVE in elastic random polycrystals,” *Journal of the Mechanics and Physics of Solids*, vol. 56, no. 9, pp. 2773–2791, 2008.
- [20] R. Hill, *The Mathematical Theory of Plasticity*. Oxford University Press, 1950.
- [21] Z. Khisaeva and M. Ostoja-Starzewski, “On the size of RVE in finite elasticity of random composites,” *Journal of Elasticity*, vol. 85, no. 2, pp. 153–173, 2006.
- [22] S. I. Ranganathan and M. Ostoja-Starzewski, “Universal elastic anisotropy index,” *Physical Review Letters*, vol. 101, no. 5, p. 055504, 2008.
- [23] M. Ostoja-Starzewski, S. Kale, P. Karimi, A. Malyarenko, B. Raghavan, S. I. Ranganathan, and J. Zhang, “Chapter two-Scaling to RVE in random media,” *Advances in Applied Mechanics*, vol. 49, pp. 111–211, 2016.
- [24] L. J. Walpole, “Elastic behavior of composite materials: theoretical foundations,” *Advances in Applied Mechanics*, vol. 21, pp. 169–242, 1981.
- [25] L. J. Walpole, “Fourth-rank tensors of the thirty-two crystal classes: multiplication tables,” in *Proceedings of the Royal Society of London A: Mathematical, Physical and Engineering Sciences*, vol. 391, no. 1800. The Royal Society, 1984, pp. 149–179.

- [26] S. I. Ranganathan, M. Ostoja-Starzewski, and M. Ferrari, “Quantifying the anisotropy in biological materials,” *Journal of Applied Mechanics*, vol. 78, no. 6, p. 064501, 2011.
- [27] M. Itskov, “On the theory of fourth-order tensors and their applications in computational mechanics,” *Computer Methods in Applied Mechanics and Engineering*, vol. 189, no. 2, pp. 419–438, 2000.
- [28] G. Holzapfel, *Nonlinear Solid Mechanics: A Continuum Approach for Engineering*. John Wiley & Sons, Ltd, 2000.
- [29] T. Kanit, S. Forest, I. Galliet, V. Mounoury, and D. Jeulin, “Determination of the size of the representative volume element for random composites: statistical and numerical approach,” *International Journal of Solids and Structures*, vol. 40, no. 13, pp. 3647–3679, 2003.
- [30] K. Sab, “On the homogenization and the simulation of random materials,” *European Journal of Mechanics-A/Solids*, vol. 11, no. 5, pp. 585–607, 1992.
- [31] C. Huet, “Application of variational concepts to size effects in elastic heterogeneous bodies,” *Journal of the Mechanics and Physics of Solids*, vol. 38, no. 6, pp. 813–841, 1990.
- [32] R. Hill, “The elastic behaviour of a crystalline aggregate,” *Proceedings of the Physical Society. Section A*, vol. 65, no. 5, pp. 349–354, 1952.
- [33] R. Quey, P. Dawson, and F. Barbe, “Large-scale 3D random polycrystals for the finite element method: Generation, meshing and remeshing,” *Computer Methods in Applied Mechanics and Engineering*, vol. 200, no. 17, pp. 1729–1745, 2011.
- [34] A. Van Pamel, G. Sha, S. Rokhlin, and M. Lowe, “Finite-element modelling of elastic wave propagation and scattering within heterogeneous media,” in *Proceedings of the Royal Society of London A: Mathematical, Physical and Engineering Sciences*, vol. 473, no. 2197. The Royal Society, 2017.
- [35] J. Zhang, Z. Chen, and C. Dong, “Simulating intergranular stress corrosion cracking in AZ31 Using three-dimensional cohesive elements for grain structure,” *Journal of Materials Engineering and Performance*, vol. 24, no. 12, pp. 4908–4918, 2015.
- [36] H. Oezelt, A. Kovacs, F. Reichel, J. Fischbacher, S. Bance, M. Gusenbauer, C. Schubert, M. Albrecht, and T. Schrefl, “Micromagnetic simulation of exchange coupled ferri-/ferromagnetic heterostructures,” *Journal of Magnetism and Magnetic Materials*, vol. 381, pp. 28–33, 2015.
- [37] M. Toifl, R. Meisels, P. Hartlieb, F. Kuchar, and T. Antretter, “3D numerical study on microwave induced stresses in inhomogeneous hard rocks,” *Minerals Engineering*, vol. 90, pp. 29–42, 2016.

- [38] P. Baudoin, V. Magnier, A. El Bartali, J.-F. Witz, P. Dufrenoy, F. Demilly, and E. Charkaluk, “Numerical investigation of fatigue strength of grain size gradient materials under heterogeneous stress states in a notched specimen,” *International Journal of Fatigue*, vol. 87, pp. 132–142, 2016.
- [39] I. Benedetti, V. Gulizzi, and V. Mallardo, “A grain boundary formulation for crystal plasticity,” *International Journal of Plasticity*, vol. 83, pp. 202–224, 2016.
- [40] M. R. Murshed and S. I. Ranganathan, “Scaling laws in elastic polycrystals with individual grains belonging to any crystal class,” *Acta Mechanica*, vol. 228, no. 4, pp. 1525–1539, 2017. [Online]. Available: <http://dx.doi.org/10.1007/s00707-016-1774-3>
- [41] C. Schumacher, B. Bickel, J. Rys, S. Marschner, C. Daraio, and M. Gross, “Microstructures to control elasticity in 3D printing,” *ACM Transactions on Graphics*, vol. 34, no. 4, p. 136, 2015.
- [42] N. Oxman, “Variable property rapid prototyping: inspired by nature, where form is characterized by heterogeneous compositions, the paper presents a novel approach to layered manufacturing entitled variable property rapid prototyping,” *Virtual and Physical Prototyping*, vol. 6, no. 1, pp. 3–31, 2011.
- [43] I. Sevostianov and M. Kachanov, “On some controversial issues in effective field approaches to the problem of the overall elastic properties,” *Mechanics of Materials*, vol. 69, no. 1, pp. 93–105, 2014.
- [44] I. Sevostianov, “On the shape of effective inclusion in the Maxwell homogenization scheme for anisotropic elastic composites,” *Mechanics of Materials*, vol. 75, pp. 45–59, 2014.
- [45] M. Jiang, K. Alzebdeh, I. Jasiuk, and M. Ostoja-Starzewski, “Scale and boundary conditions effects in elastic properties of random composites,” *Acta Mechanica*, vol. 148, no. 1-4, pp. 63–78, 2001.
- [46] S. Kale, A. Saharan, S. Koric, and M. Ostoja-Starzewski, “Scaling and bounds in thermal conductivity of planar gaussian correlated microstructures,” *Journal of Applied Physics*, vol. 117, no. 10, p. 104301, 2015.
- [47] M. Ostoja-Starzewski and J. Schulte, “Bounding of effective thermal conductivities of multiscale materials by essential and natural boundary conditions,” *Physical Review B*, vol. 54, no. 1, pp. 278–285, 1996.
- [48] Z. Khisaeva and M. Ostoja-Starzewski, “Mesoscale bounds in finite elasticity and thermoelasticity of random composites,” in *Proceedings of the Royal Society of London A: Mathematical, Physical and Engineering Sciences*, vol. 462, no. 2068, 2006, pp. 1167–1180.

- [49] M. Karim and K. Krabbenhoft, “Extraction of effective cement paste diffusivities from X-ray microtomography scans,” *Transport in Porous Media*, vol. 84, no. 2, pp. 371–388, 2010.
- [50] M. Ostoja-Starzewski and S. I. Ranganathan, “Scaling and homogenization in spatially random composites,” *Mathematical Methods and Models in Composites. Imperial College Press, London*, pp. 61–101, 2013.
- [51] S. I. Ranganathan and M. Ostoja-Starzewski, “Scale-dependent homogenization of inelastic random polycrystals,” *Journal of Applied Mechanics*, vol. 75, no. 5, p. 051008, 2008.
- [52] M. Ostoja-Starzewski, “Scale effects in plasticity of random media: status and challenges,” *International Journal of Plasticity*, vol. 21, no. 6, pp. 1119–1160, 2005.
- [53] M. Jiang, M. Ostoja-Starzewski, and I. Jasiuk, “Scale-dependent bounds on effective elastoplastic response of random composites,” *Journal of the Mechanics and Physics of Solids*, vol. 49, no. 3, pp. 655–673, 2001.
- [54] F. El Houdaigui, S. Forest, A.-F. Gourgues, and D. Jeulin, “On the size of the representative volume element for isotropic elastic polycrystalline copper,” in *IUTAM Symposium on Mechanical Behavior and Micro-Mechanics of Nanostructured Materials*. Springer, 2007, pp. 171–180.
- [55] A. S. Dalaq, S. I. Ranganathan, and M. Ostoja-Starzewski, “Scaling function in conductivity of planar random checkerboards,” *Computational Materials Science*, vol. 79, pp. 252–261, 2013.
- [56] J. Zhang and M. Ostoja-Starzewski, “Frequency-dependent scaling from mesoscale to macroscale in viscoelastic random composites,” in *Proceedings of the Royal Society of London A: Mathematical, Physical and Engineering Sciences*, vol. 472, no. 2188, 2016.
- [57] J. G. Berryman, “Bounds and self-consistent estimates for elastic constants of random polycrystals with hexagonal, trigonal, and tetragonal symmetries,” *Journal of the Mechanics and Physics of Solids*, vol. 53, no. 10, pp. 2141–2173, 2005.
- [58] J. P. Watt, “Hashin-Shtrikman bounds on the effective elastic moduli of polycrystals with monoclinic symmetry,” *Journal of Applied Physics*, vol. 51, no. 3, pp. 1520–1524, 1980.
- [59] D. R. Lide, *Handbook of Chemistry and Physics*. CRC Press, 2004.
- [60] J. M. Brown, R. J. Angel, and N. Ross, “Elasticity of plagioclase feldspars,” *Journal of Geophysical Research: Solid Earth*, vol. 121, pp. 663–675, 2016.

- [61] J. P. Watt and L. Peselnick, “Clarification of the Hashin-Shtrikman bounds on the effective elastic moduli of polycrystals with hexagonal, trigonal, and tetragonal symmetries,” *Journal of Applied Physics*, vol. 51, no. 3, pp. 1525–1531, 1980.
- [62] H. Ledbetter and S. Kim, “Monocrystal elastic constants and derived properties of the cubic and the hexagonal elements,” *Handbook of Elastic Properties of Solids, Liquids and Gases*, vol. 2, pp. 97–106, 2001.
- [63] K. Bhattacharya and P. Suquet, “A model problem concerning recoverable strains of shape-memory polycrystals,” in *Proceedings of the Royal Society of London A: Mathematical, Physical and Engineering Sciences*, vol. 461, no. 2061, 2005, pp. 2797–2816.
- [64] M. R. Murshed and S. I. Ranganathan, “Hill-Mandel condition and bounds on lower symmetry elastic crystals,” *Mechanics Research Communications*, vol. 81, pp. 7 – 10, 2017. [Online]. Available: <http://dx.doi.org/10.1016/j.mechrescom.2017.01.005>
- [65] C. M. Kube and A. P. Arguelles, “Bounds and self-consistent estimates of the elastic constants of polycrystals,” *Computers & Geosciences*, vol. 95, pp. 118–122, 2016.
- [66] W. Voigt, “Lehrbuch der kristallphysik (mit ausschluss der kristalloptik),” *Leipzig–Berlin: BG Teubner*, 1928.
- [67] A. Reuss, “Berechnung der fließgrenze von mischkristallen auf grund der plastizitätsbedingung für einkristalle.” *ZAMM-Journal of Applied Mathematics and Mechanics/Zeitschrift für Angewandte Mathematik und Mechanik*, vol. 9, no. 1, pp. 49–58, 1929.
- [68] Z. Hashin and S. Shtrikman, “A variational approach to the theory of the elastic behaviour of polycrystals,” *Journal of the Mechanics and Physics of Solids*, vol. 10, no. 4, pp. 343–352, 1962.
- [69] A. Norris, “An examination of the Mori-Tanaka effective medium approximation for multiphase composites,” *Journal of Applied Mechanics*, vol. 56, no. 1, pp. 83–88, 1989.
- [70] J. M. Brown, “Determination of Hashin–Shtrikman bounds on the isotropic effective elastic moduli of polycrystals of any symmetry,” *Computers & Geosciences*, vol. 80, pp. 95–99, 2015.
- [71] S. I. Ranganathan, M. R. Murshed and L. Costa, “Heterogeneous anisotropy index and scaling in two-phase random polycrystals,” *under minor revision*, 2017.

- [72] M. Sledzinska, B. Graczykowski, M. Placidi, D. S. Reig, A. El Sachat, J. Reparaz, F. Alzina, B. Mortazavi, R. Quey, L. Colombo *et al.*, “Thermal conductivity of MoS₂ polycrystalline nanomembranes,” *2D Materials*, vol. 3, no. 3, p. 035016, 2016.
- [73] M. Ardeljan, I. J. Beyerlein, and M. Knezevic, “A dislocation density based crystal plasticity finite element model: Application to a two-phase polycrystalline HCP/BCC composites,” *Journal of the Mechanics and Physics of Solids*, vol. 66, pp. 16–31, 2014.
- [74] Z. Hashin and S. Shtrikman, “A variational approach to the theory of the elastic behaviour of multiphase materials,” *Journal of the Mechanics and Physics of Solids*, vol. 11, no. 2, pp. 127–140, 1963.
- [75] L. J. Walpole, “On the overall elastic moduli of composite materials,” *Journal of the Mechanics and Physics of Solids*, vol. 17, no. 4, pp. 235–251, 1969.
- [76] J. P. Watt, G. F. Davies, and R. J. O’Connell, “The elastic properties of composite materials,” *Reviews of Geophysics*, vol. 14, no. 4, pp. 541–563, 1976.
- [77] T. Mori and K. Tanaka, “Average stress in matrix and average elastic energy of materials with misfitting inclusions,” *Acta Metallurgica*, vol. 21, no. 5, pp. 571–574, 1973.
- [78] Y. Benveniste, “A new approach to the application of Mori-Tanaka’s theory in composite materials,” *Mechanics of Materials*, vol. 6, no. 2, pp. 147–157, 1987.
- [79] G. Weng, “The theoretical connection between Mori-Tanaka’s theory and the Hashin-Shtrikman-Walpole bounds,” *International Journal of Engineering Science*, vol. 28, no. 11, pp. 1111–1120, 1990.
- [80] Y. Ni and M. Y. Chiang, “Prediction of elastic properties of heterogeneous materials with complex microstructures,” *Journal of the Mechanics and Physics of Solids*, vol. 55, no. 3, pp. 517–532, 2007.
- [81] J. D. Eshelby, “The determination of the elastic field of an ellipsoidal inclusion, and related problems,” in *Proceedings of the Royal Society of London A: Mathematical, Physical and Engineering Sciences*, vol. 241, no. 1226. The Royal Society, 1957, pp. 376–396.
- [82] M. Ostoja-Starzewski, L. Costa, and S. I. Ranganathan, “Scale-dependent homogenization of random hyperbolic thermoelastic solids,” *Journal of Elasticity*, vol. 118, no. 2, pp. 243–250, 2015.
- [83] T. Kanit, F. N’Guyen, S. Forest, D. Jeulin, M. Reed, and S. Singleton, “Apparent and effective physical properties of heterogeneous materials: representativity of samples of two materials from food industry,” *Computer Methods in Applied Mechanics and Engineering*, vol. 195, no. 33, pp. 3960–3982, 2006.

- [84] K. Norian, “Equivalent circuit components of nickel-cadmium battery at different states of charge,” *Journal of Power Sources*, vol. 196, no. 11, pp. 5205–5208, 2011.
- [85] Y. Wang, K. H. Lu, V. Gupta, L. Stiborek, D. Shirley, S.-H. Chae, J. Im, and P. S. Ho, “Effects of Sn grain structure on the electromigration of Sn–Ag solder joints,” *Journal of Materials Research*, vol. 27, no. 08, pp. 1131–1141, 2012.
- [86] I. H. Kazi, P. Wild, T. Moore, and M. Sayer, “Characterization of sputtered nichrome (Ni–Cr 80/20 wt.%) films for strain gauge applications,” *Thin Solid Films*, vol. 515, no. 4, pp. 2602–2606, 2006.
- [87] M. Srivastava, V. E. Selvi, V. W. Grips, and K. Rajam, “Corrosion resistance and microstructure of electrodeposited nickel-cobalt alloy coatings,” *Surface and Coatings Technology*, vol. 201, no. 6, pp. 3051–3060, 2006.
- [88] S. I. Ranganathan and M. R. Murshed, “Scaling function in mechanics of random materials,” *Encyclopedia of Continuum Mechanics*, accepted, 2017.
- [89] F. M. White, *Fluid Mechanics*. McGraw-Hill, New York, 2003.
- [90] J. Kuneš, *Dimensionless Physical Quantities in Science and Engineering*. Elsevier, 2012.
- [91] S. N. Shore, *An Introduction to Astrophysical Hydrodynamics*. Academic Press, 2012.
- [92] R. Splinter, *Handbook of Physics in Medicine and Biology*. CRC Press, 2010.
- [93] S. I. Ranganathan, P. Decuzzi, L. T. Wheeler, and M. Ferrari, “Geometrical anisotropy in biphasic particle reinforced composites,” *Journal of Applied Mechanics*, vol. 77, no. 4, p. 041017, 2010.
- [94] S. I. Ranganathan, D. M. Yoon, A. M. Henslee, M. B. Nair, C. Smid, F. K. Kasper, E. Tasciotti, A. G. Mikos, P. Decuzzi, and M. Ferrari, “Shaping the micromechanical behavior of multi-phase composites for bone tissue engineering,” *Acta Biomaterialia*, vol. 6, no. 9, pp. 3448–3456, 2010.
- [95] L. Gorb, V. Kuz'min, and E. Muratov, *Application of Computational Techniques in Pharmacy and Medicine*. Springer, 2014, vol. 17.
- [96] J. Donea and A. Huerta, *Finite Element Methods for Flow Problems*. John Wiley & Sons, 2003.
- [97] P. K. Panigrahi, *Transport Phenomena in Microfluidic Systems*. John Wiley & Sons, 2016.
- [98] K. H. Huebner, D. L. Dewhurst, D. E. Smith, and T. G. Byrom, *The Finite Element Method for Engineers*. John Wiley & Sons, 2008.

- [99] T. Mukherjee, V. Manvatkar, A. De, and T. DebRoy, “Dimensionless numbers in additive manufacturing,” *Journal of Applied Physics*, vol. 121, no. 6, p. 064904, 2017.
- [100] P.-S. Koutsourelakis, “Stochastic upscaling in solid mechanics: An exercise in machine learning,” *Journal of Computational Physics*, vol. 226, no. 1, pp. 301–325, 2007.
- [101] M. Rupp, A. Tkatchenko, K.-R. Müller, and O. A. Von Lilienfeld, “Fast and accurate modeling of molecular atomization energies with machine learning,” *Physical Review Letters*, vol. 108, no. 5, p. 058301, 2012.
- [102] M. Rupp, “Machine learning for quantum mechanics in a nutshell,” *International Journal of Quantum Chemistry*, vol. 115, no. 16, pp. 1058–1073, 2015.

Appendix

Author's Biography

Ridwan was born in Dhaka, Bangladesh and he completed his schooling from Arab Unity School, Dubai, United Arab Emirates (UAE). He obtained a bachelor's degree in mechanical engineering with a minor in aerospace engineering from American University of Sharjah, Sharjah, UAE. Prior to starting his master's at Rowan University, he worked as a Mechanical Engineer at Petrofac, Sharjah. He completed his master's degree in mechanical engineering from Rowan University and his master's thesis was titled 'Design Maps For Fracture Resistant Functionally Graded Materials'.

Ridwan has won several awards and scholarships in undergraduate as well as graduate education including the Chancellor's List Award, Dean's List Award, Merit Scholarship for eight successive semesters (Fall 2009 to Spring 2013), Certificate of Recognition by Shell Oil Company, Graduate Teaching Fellowship Award for Master's, Graduate Research Fellowship Award for Ph.D., Alpha Epsilon Lambda National Graduate Honor Society, President's Scholar of Excellence (CGPA: 4.0/4.0) and Graduate Dean's List Award for five consecutive semesters (Spring 2015 to Spring 2017). In addition, Ridwan has contributed to the design of a prototype vehicle (Eco-Stallion) and the Smart Orthopaedic Implants that received wide-spread media coverage.

Ridwan's research interests are broadly in the areas of applied mechanics, namely computational multiscale mechanics, computational fracture mechanics and orthopaedic biomechanics. During his stay at Rowan, Ridwan has published in several leading engineering and medical journals including European Journal of Mechanics-A/Solids, Acta Mechanica, Mechanics Research Communications, Encyclopedia of Continuum Mechanics and Medical Hypotheses.